MULTI-HAZARD RESPONSE CHARACTERIZATION OF TALL BUIDINGS

A Thesis

by

KARTHIKA RAMESH

Submitted to the Office of Graduate and Professional Studies of
Texas A&M University
in partial fulfillment of the requirements for the degree of

MASTER OF SCIENCE

Chair of Committee,	John Niedzwecki
Co-Chair of Committee,	Luciana Barroso
Committee Member,	H. Joseph Newton
Head of Department,	Robin Autenrieth

August 2016

Major Subject: Civil Engineering

ABSTRACT

The series of recent extreme weather events and subsequent damage to the infrastructure has led to an increased concern regarding the design of structural systems for multi-hazard criteria. Since much of the multi-storied infrastructure of the twentieth century exceeds nearly fifty years of service, innovative instrumentation of buildings has attracted a great deal of research attention. These increased environmental concerns coupled with the increasing population density result in the operational demand on these structures far exceeding their original design criteria or capacity.

This research addresses the response characterization of tall building structures subject to strong ground motion and wind loading. The time history of various building designs is developed using a finite element idealization of the building subject to various environmental loading scenarios. The resulting time series of the response behavior is obtained at each building floor elevation. The characterization of response behavior is analyzed using the Time Domain Decomposition (TDD) method, which requires no prior assumptions about the nature of time series or the excitation. TDD's application is first studied on a 20-story building where the first three translational and rotational modes are examined. The analysis is then extended to a more flexible 52-story idealized version of a prototype of the Prudential Tower located in Boston, Massachusetts. This research study investigates the reconstruction of response time series for arrays of sensors located at various floor elevations recognizing that sensor failure may occur and that some information may be lost.

The sensor configurations presented are used to illustrate some of the intricacies involved in the application of the TDD method that affect the accuracy of the reconstruction of time domain response behavior. The interpretation of data based upon modal filtering was demonstrated to influence the process of signal reconstruction, complicating the relationship between the number of sensors and the modal information. Further, it was observed that the response behavior due to wind loading, which is basically a unidirectional load varying with both elevation and time, when compared with that from the bidirectional seismic loading case is quite different although they excite similar modal frequencies. The insights gained from this study help to quantify the role of sensor placement on tall buildings that are subject to regional multi-hazard loading that will vary in terms of both the nature and intensity of dynamic excitation. The research study also identified deficiencies in the underlying methodology that need further investigation to improve the robustness of this approach as a tool for dynamic response characterization.

DEDICATION

To my beloved parents and teachers.

ACKNOWLEDGEMENTS

I would like to extend my gratitude towards my committee chair, Dr. John Niedzwecki, for his able guidance and encouragement throughout the course of this research. I would also like to thank my committee members, Dr. Luciana Barroso for her constant support and motivation and Dr. Joseph Newton, for his valuable inputs. My graduate education would not have been possible without the financial support given by the Department of Industrial Distribution. I profusely thank Dr. Barry Lawrence and Mr. Bharani Nagarathnam for graciously providing me a graduate assistantship with an extremely conducive work atmosphere from the first day of study.

I am very grateful to my friends and peers particularly Mr. Amritansh Parth, Mr. Maysam Kiani, Ms. Jackeline Kafie-Martinez and Mr. Ruthwik Lakshman for providing an ear to all my problems. I also extend my gratitude to the faculty and staff at the Zachery Department of Civil Engineering for making my time at Texas A&M University a wonderful and enriching experience. I would also like to thank my uncle Mr. Ramesh Krishnamurthi a former Aggie who inspired and enabled my journey to Texas A&M.

Finally, I would like to thank my parents and my brother for having supported me through all endeavors in life.

TABLE OF CONTENTS

LIST OF FIGURES

LIST OF TABLES

1. INTRODUCTION

1.1 Background and motivation

Structural life extension and health monitoring have become major areas of study in the past few decades, however it still remains a technically challenging task to monitor tall structures and interpret the measurements obtained. In particular, a significant portion of the country's aging multi-storied infrastructure is located in densely populated metropolitan areas. This is especially a concern as the design codes used to design these structures did not consider their increased usage by a growing population nor the climatic concerns that threaten to escalate the risks of natural hazards in the years to come. Since a vast majority of the monitoring systems are based on externally attached sensors, there is a much higher threat of sensor failure during a disaster. Moreover, in tall multi-storied buildings, it is not reasonable to have sensors installed on every building floor; hence the issue of sensor failure is an additional concern that also needs to be addressed. Other important requirements include ability of the sensor network to function on low power and durability to withstand long-term vibrational loading. Sensor network design and experimental testing in conjunction with elaborate finite element modelling is required to determine its performance. Figure 1.1 illustrates the instrumentation in place at The Landmark, Abu Dhabi a 1063ft skyscraper with 72 floors. It can be observed that the number of sensors is significantly lesser than the floor count especially with regards to the dynamic monitoring system.

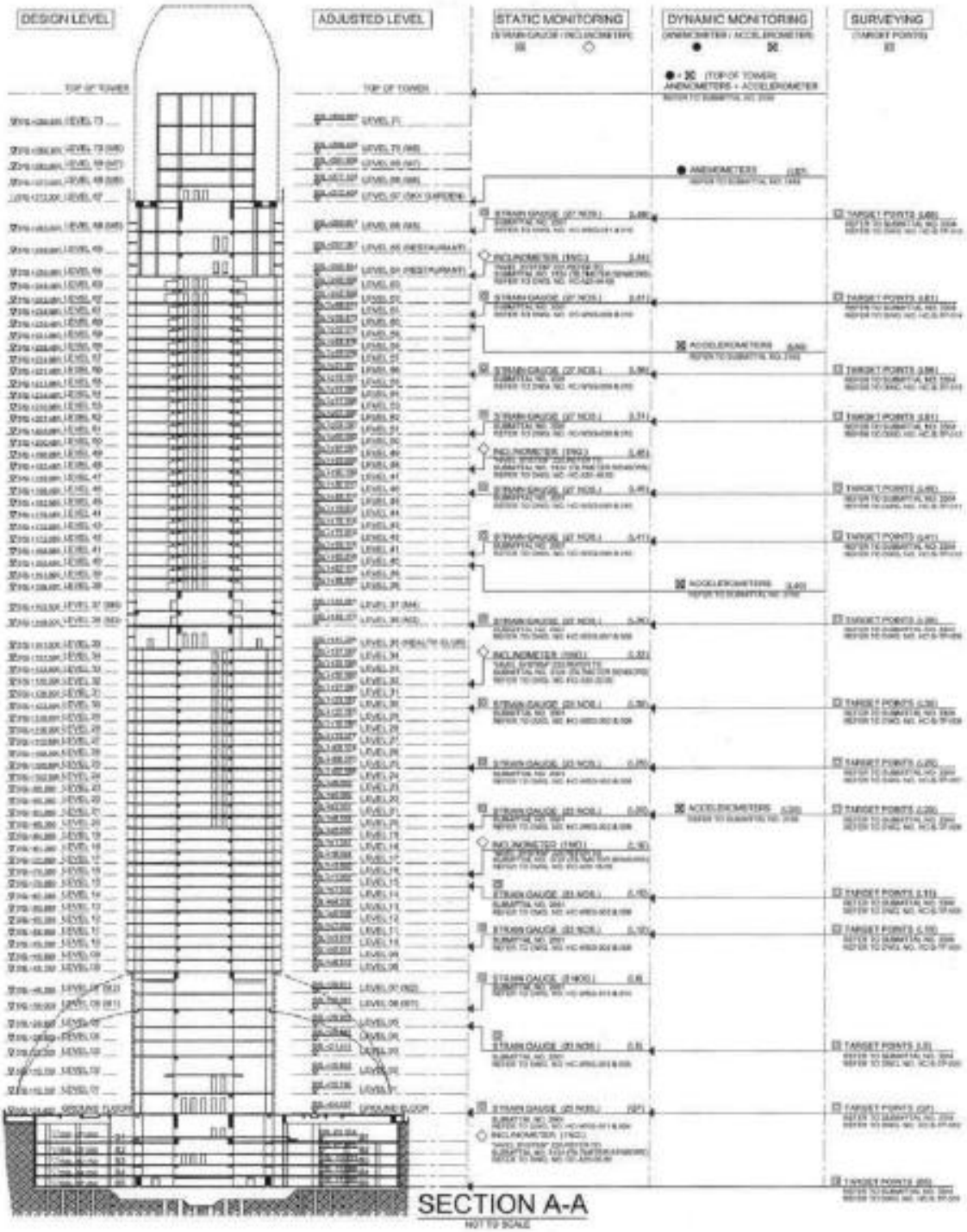

Figure 1.1 Instrumentation in The Landmark, Abu Dhabi [27]

Obtaining the structural response for an extreme event requires a sampling strategy to focus on the analysis of data from that single event. This is imperative as these events are usually seasonally dependent and the volume of data collected over the service life of a structure will be enormous. Such a strategy should focus on sensor type and network selection, placement of recording stations and analysis of the recorded data to derive the required response. This response can then be used as a basis for assessing the importance of missing response information needed to evaluate structural health.

This research explores dynamic response characterization of tall buildings to strong ground motion and wind loads. The structural response is characterized using the Time Domain Decomposition method (TDD), a modal extraction technique originally proposed in 2005 by Kim, Stubbs and Park [16]. The TDD methodology was initially applied to data obtained from equally spaced sensor measurements on a bridge structure. Its application was later extended to modal extraction and response reconstruction of unequally spaced biaxial accelerometer and fiber optic strain measurements in long flexible horizontal cylinders in a series of studies reported by Niedzwecki and Fang ([8], [24], [25]).

The TDD methodology has been adopted in this research as it has several interesting characteristics for the analysis of data obtained from sensor arrays. The technique utilizes ambient excitation for modal analysis unlike other decomposition methods, which require free decay response. In addition, the resolution of modal information is directly proportional to the number of sensors, which results in minimizing computational complexity and effort. Moreover, the procedure requires no

assumptions with regards to the nature of excitation, structural response, or any modal information *a priori*. Reconstruction of original time series can also be performed using the modal results, which can also serve as a means to evaluate the adequacy of the sensor array.

1.2 Research objectives and approach

The primary objective of this research is to explore the wealth of information embedded within the dynamic structural response of multi-storied buildings. In particular, the focus is on deriving the structure's modal characteristics and investigating response reconstruction using limited sensor data. Since, sensor network selection and placement is an important aspect of the problem discussed, a literature survey of recent practices in sensor technology and structural control strategies were pursued as part of the thesis research. It was however not possible to gather sensor data directly from instrumented buildings as part of this study. Thus, the study involved the selection of strong ground motion data and wind simulation models available in the open literature. The buildings used in this study were modeled using the finite element framework of SAP 2000 [30] and resulting models were used as the basis to generate the necessary response time histories used as input for the TDD analysis.

This thesis is organized into seven chapters. The first chapter serves to provide a context for multi-hazard response recording of multi-storied structures and introduces the TDD methodology used for the response characterization process. The second chapter highlights the impact of the monitoring systems for response characterization and presents a survey of the state of the art developments in relevant sensor types, sensor

placement technologies and structural control strategies. The third chapter provides a detailed account of the mathematical formulation behind the TDD methodology. The fourth chapter presents a preliminary analysis, employing the TDD technique purely for the purpose of modal extraction, from the seismic response histories of a 20-story building that have previously been reported in the open literature. The fifth chapter presents a discussion of the modal characteristics of tall and super tall structures to understand their dynamic properties and serve as means to develop an idealized building to further explore the applicability of the TDD methodology. The sixth chapter presents the results of response reconstruction for a simplified 52-story building partially resembling the Prudential Tower in Boston Massachusetts. The seventh and final chapter presents the summary and conclusions of this thesis.

2. SURVEY OF SENSOR SYSTEMS AND CONTROL STRATEGIES

The response recording system plays a significant role towards response characterization by affecting the properties of parameters derived from it. Response sensitivity and hence the characterization accuracy is governed by the type of sensing network, while the number and location of sensors control the quality and quantity of derivable modal characteristics. The sensing network may also be equipped to support damping devices that can control the magnitude of measured response and in turn alter its response behavior. Apart from these features, the general setup of the sensor network including its functionality during a catastrophic event, power requirements, data transmission system, adaptability to different media (concrete, steel and timber structures), ease of installation and maintenance also govern the quality of recorded response and therefore its response characterization. Thus it is essential to first understand some of the current research in sensor technology and in particular, sensor types, measurements techniques, sensor placement and optimization to structural control systems.

2.1 Sensor types and measurement techniques

Researchers are exploring a wide range of instrumentation, measurement and analysis technologies employed to accurately measure both the environmental excitation and structural response. They are incorporating a wide range of technologies in their research that includes laser technology, fiber optics, wireless sensing, advanced vision based measurements, innovative smart paint sensors and piezo-ceramic sensing

aggregates with the objective of achieving suitable signal processing and measurement sensitivity. A synopsis of select sensor types capable of dynamic response measurement is provided at the end of this section in a tabular form (Table 2.1) and a more detailed description of their functionality is discussed here.

Laser technology and laser based Fiber Bragg gratings (FBGs), have gained more prominence in recent years owing to FBG's ability of reflecting optical radiation around a specific wavelength. Fiber optics in general is found to display several advantages such as no electrical power requirement (utilizes low power infra-red laser source), robustness at elevated temperatures, low signal losses (0.2 dB/km), multiplexing ability (allowing multiple sensors to be operated from a single signal conditioning unit), small size and immunity to electromagnetic interference [15]. Gagliardi et al. [9] have developed an optical FBG accelerometer based on a semiconductor diode-laser source for measuring horizontal ground motions. Plane acceleration components of the sensor's mass are detected by two fiber Bragg gratings anchored to it. The sensor is found to exhibit an operational range of up to 30 Hz and exhibits sensitivity comparable with the state of the art devices. Górriz, García, Payá-Zaforteza and Maicas [12] have proposed hybrid FBG long gauge sensors to measure displacements in non-homogeneous media such as concrete and wood. Unlike the traditional short gauge sensors, their long gauge counterparts give the mean strain value between two points far enough apart to not be influenced by local irregularities. The sensor is anchored to the host using a two-component adhesive with an elasticity greater than 400 MPa to allow transmission of strains. Experimental testing of concrete specimens subjected to compression loading

and unloading cycles revealed that the sensor may fail due to shear forces in the anchorage zone or due to buckling. Compared to other fiber optic sensors, it carries the advantage that prestressing of the optical fiber is not required in this case. More recently Kim and Kim [17] have developed a Terrestrial laser scanner (TLS) that acquires the horizontal distance and time stamp of an object by repeatedly aiming laser beams at an identical point using its line scan mode. The time stamp is then used to synchronize the dataset. Optimal weighted averaging is adopted to combat the high inherent noise contamination in the measurements.

Another domain of extensive investigation is wireless sensor networks (WSNs) for ease of installation and data transfer. Mascarenas et al. [22] have come up with capacitance and impedance based wireless sensors and sensor nodes for use in wireless networks. These sensor nodes are designed to be triggered as required by means of an unmanned mobile host that generates a Radio Frequency (RF) signal near the receiving antennas connected to them. Measured response is transmitted back to the mobile host by means of a wireless system. Two types of sensor nodes are developed for this purpose both of which require very low power. The Capacitance-based nodes collect peak displacement measurements while the Impedance based nodes collect electromechanical impedance data. A schematic of the proposed network is shown in Figure 2.1. The Rectannas are the rechargeable batteries/capacitors which draw power from the mobile host and supply it to the sensing network attached to it. Qiu, Wu and Yuan [29] have proposed a cluster start wireless network for strain gauge sensor nodes to synchronously gather, process and transmit signals. A multi-point network evaluation

system has also been developed for testing. It was observed that an increase in the strain monitoring points complicates the network design and requires superior data processing capacity.

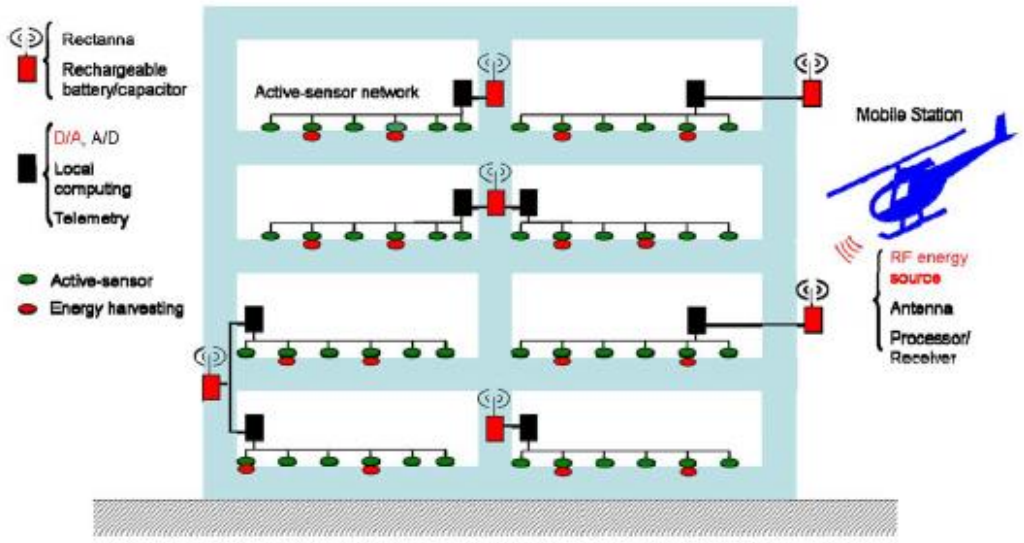

Figure 2.1 Mobile host based sensing networks [22]

Other innovative sensor networks include, for example, an advanced vision based system that is a unique non-contact-type method developed by Lee, Ho, Shinozuka and Lee [20] using the partitioning approach requiring cameras with 30 frames per second. Response is successively estimated from multiple sub-systems that capture and process images using camcorders connected to secondary processing computers. Data is then wirelessly transferred to the primary system using the TCP/IP (Transmission Control protocol/Internet Protocol) protocol. Static and dynamic tests were carried out on three and five story steel buildings where errors of less than 2.0% were observed between the

test results and direct measurements. Liao et al. [21] have proposed water proofed Piezo-ceramic-based sensors (PZT) that can be pre-embedded as 'smart aggregates' or post embedded in reinforced concrete columns subjected to seismic loads. The choice of material (piezo-ceramic) is due to its advantageous properties such as active sensing, quick response, low cost, simplicity in implementation and availability in different shapes. Post embedded PZTs are placed in drilled holes refilled by non-shrinkage mortar. Shake table testing of a reinforced concrete (RC) column and *in-situ* experimental testing of the RC piers of Niu-Dou Bridge, Taiwan to seismic loading revealed that a smart aggregate located in the middle of a column behaves as an actuator while the ones at the top and bottom portions behave as sensors. Wavelet packet analysis was used to analyze the signals detected by the smart aggregates.

Al-Saffar, Aldraihem and Baz [1] have developed smart paint sensors that are installed as a narrow band of coating along the central transverse portion of a thin strip attached to the specimen to be monitored. The paint is manufactured from an epoxy resin mixed with Carbon Black nano-particles to gain electrical conductivity and sensitivity to mechanical excitations. Such paints have gained attention, as they possess attractive attributes of both polymers and the piezoelectric particles. The sensor has only been tested in a one-dimensional domain, on a beam structure. A multi-field model is developed by integrating the sensor equations with the finite element model of the base beam and subjecting the system to several vibration excitations. Predictions from this model are then validated experimentally. Results indicate that the sensitivity of the paint sensor is found to be comparable to that of conventional strain gages.

Meng and Ansari [23] have experimented with a fiber optic low frequency tiltmeter, which is primarily a sensitive equipment used for measuring small changes in the vertical level. The tiltmeter design consists of a thin cantilever beam with a mass at the free end. For the purpose of simplicity, the mass of the beam is considered to be negligible and the mass block is treated as a lumped mass. The sensor rotation is correlated against the cantilever's end strain developed due to the force exerted by the lumped mass. The system also includes a damping fluid to control the dynamic response. Two symmetrically placed FBGs are used for cancelling thermal effects hence achieving temperature compensation. The tiltmeter is found to exhibit linearity over a range of measurements common in low-frequency vibrations of bridges with a measurement resolution of 0.005deg. The damped system shows phase stability even at higher rates of displacement. Appropriate selection of materials and right proportioning of the beam- lumped mass system can achieve high sensitivity.

Table 2.1 Summary of sensor types and measurement techniques

Sensor type	Authors	Measurement approach	Testing and conclusions	Other notable points
Laser based optical Fiber Bragg- Grating accelerometer [9]	Gagliardi et al., 2008	System is based on a semiconductor diode-laser source that interrogates a two-dimensional inertial sensor suitable for measurement of horizontal ground accelerations.	Experimental testing: Shake table test Shows good performance when compared to a commercial 'Episensor' accelerometer Exhibits an operational range up to 30Hz and a dynamics of about 100dB, with a sensitivity comparable to state-of-the-art devices.	Plane acceleration components of the sensor's mass are detected by two Fiber Bragg-Gratings (FBGs) anchored to its structure.
Capacitance based and impedance based wireless sensors and sensor nodes [22]	Mascarenas et al., 2009	An unmanned mobile host node is used to generate a Radio Frequency (RF) signal near receiving antennas connected to sensor nodes embedded on the structure to be monitored. Measured response is transmitted back from sensors to the mobile host via a wireless system.	Experimental testing: Alamosa Canyon Bridge Sensor nodes require very low-power Nodes are capable of being wirelessly triggered by the mobile agent as required	Two types of wireless sensor nodes are developed. Capacitance-based: To collect peak displacement measurements Impedance based: To collect electromechanical impedance data.
Wireless sensor network [29]	Qiu, Wu & Yuan, 2011	A cluster start network is deployed to synchronously gather, process and transmit strain gauge signals from precision strain sensor nodes.	Experimental testing: Aircraft structure An increase in the strain monitoring points complicates the network design and requires superior data processing capacity.	A multi-point network evaluation system is developed for the testing.

Table 2.1 Continued

Sensor type	Authors	Measurement approach	Testing and conclusions	Other notable points
Piezoceramic-based sensors (PZT) [21]	Liao et al., 2011	Water proofed PZTs are either pre -embedded as 'smart aggregates' or post embedded in RC columns subjected to seismic loads.	Experimental testing: RC piers of Niu-Dou Bridge, Taiwan A smart aggregate located in the middle of a column behaves as an actuator while the ones at the top and bottom portions behave as sensors.	Wavelet packet analysis was used to analyze the signals detected by the smart aggregates.
Smart paint sensors [1]	Al-Saffar, Aldraihem & Baz, 2012	Sensor is installed as a narrow band of coating along the central transverse portion of a thin strip attached to the specimen to be monitored.	Experimental testing: Cantilever beam Numerical modelling : 1-D FEM model based on Bernoulli–Euler beam theory Sensitivity is found to be comparable to that of conventional strain gages.	Sensor is manufactured from an epoxy resin mixed with Carbon Black nano-particles to gain electrical conductivity and sensitivity to mechanical excitations.
Advanced vision based system [20]	Lee, Ho, Shinozuka & Lee, 2012	Measurement uses the partitioning approach. Response is successively estimated from multiple sub-systems that capture and process images using camcorders and computers. This and the time synchronization information are then wirelessly transferred to the master system using the TCP/IP protocol.	Experimental testing: Static and dynamic tests on three and five story steel buildings Errors of less than 2.0% were observed between test results and direct measurements.	Measurement points can be expanded at the secondary level using commercial devices. Cameras with 30 frames per second are required for displacement monitoring

Table 2.1 Continued

Sensor type	Authors	Measurement approach	Testing and conclusions	Other notable points
Damped fiber optic low frequency tiltmeter [23]	Meng & Ansari, 2013	The tiltmeter consists of a thin cantilever beam with a mass block at the free end. Cantilever end strain due to the force exerted by the lumped mass is correlated against the sensor rotation. Design includes a damping fluid to control dynamic response.	Tiltmeter exhibits linearity over a range of measurements common in low-frequency vibrations of bridges. A measurement resolution of 0.005deg is obtained. The damped system shows phase stability at higher rates of displacements.	High sensitivity can be achieved by the appropriate selection of materials and right proportioning of the beam- lumped mass system. Two symmetrically placed FBGs are used for cancelling thermal effects hence achieving temperature compensation.
Hybrid FBG long gauge sensor [12]	Górriz, García, Payá-Zaforteza & Maicas, 2014	Sensor is anchored to the host using a two-component adhesive with an elasticity modulus greater than 400MPa to allow transmission of strains. It does not require prestressing of the optical fiber.	Experimental testing: Concrete specimens subjected to compression loading–unloading cycles. Sensor may fail due to shear forces in the anchorage zone or due to buckling.	An FBG is a reflector built in a short segment of the core of an optical fiber by exposing it to intense UV light.
Terrestrial laser scanner (TLS) [17]	Kim & Kim, 2015	TLS's line scan mode is used to repeatedly aim laser beams at an identical point to acquire its horizontal distance and time stamp. The dataset is synchronized based on the obtained time stamp.	Experimental testing: Cantilever beam There is high inherent noise contamination in the measurements. Optimal weighted averaging is adopted to combat this.	Distances are measured using the Time of flight method. (Laser beam's travel time multiplied by speed). Not all TLSs have the option of line scanning.

2.2 Sensor placement and optimization

The decision on the type of sensor required should then be followed by the decision on the number and location of sensors to be used. Multi-type sensors are required to measure not only global structural response but also local stresses and strains to assess the entire structural performance. Hence, optimal sensor placement for the best reconstruction of structural responses required in areas of sensor failure or absence is an important task studied widely in the literature. Some of the prominent methods used in this domain include clustering algorithms, transmissibility matrix generation, and Kalman filtering. Their testing is however restricted to beams, trusses and small framed systems. A summary of pertinent research practices is presented in Table 2.2 given at the end of this section and a more detailed discussion follows below.

Wang, Wei and Sun [30] have proposed a sample selection based on kernel sub-clustering for the signal reconstruction of multifunctional sensors. A Kernel function is a generalization of the distance metric obtained by mapping data, which are non-separable in the original space, into homogeneous groups in the high-dimensional space. The method calculates distance between two data points based on the kernel-induced distance instead of the conventional distance. More recently, Wang, Law and Yang [29] have developed a two-step reconstruction method based on the transmissibility matrix between two sets of sensor locations. The initial sensor combination is obtained by singular value decomposition of a re-assembled Markov parameter matrix corresponding to all candidate sensor locations. The final sensor placement is then decided by minimization of a measurement noise effect index using a heuristic forward sequential

sensor placement algorithm. Numerical modelling shows that the resulting sensor placement model produces responses with acceptable errors even with five percent measurement noise.

Zhang and Xu [32] have come up with a reconstruction algorithm based on the framework of Kalman filter with unknown excitation. The method is independent of the type and time evolution of external excitation. Reconstruction is done by extending the simultaneous input and state estimation of a linear stochastic system. Oh et al. [22] have developed a strain measurement model using a limited number of sensors for steel beam structures subjected to uncertain loadings. Unknown strains are obtained from a general form equation derived using the known limited sensor data. This method can also be used to derive the optimal number of sensors required. The method is a good fit for single span beams while for multi span beams with limited sensors large errors were observed. Estimations of strain distributions are influenced by loading condition, order of approximation function, number and location of sensors.

Table 2.2 Summary of sensor placement and optimization

Title	Authors	Approach	Testing and conclusions	Other notable points
Sample selection based on kernel-subclustering for the signal reconstruction of multifunctional sensors. [30]	Wang, Wei & Sun, 2012	Method is based on kernel-subclustering distill groupings of the sample data. It calculates the distance between two data points based on the kernel-induced distance instead of the conventional distance.	The simulation results show greater accuracy with fewer selected points than other clustering methods in the literature.	Kernel function is a generalization of the distance metric obtained by mapping data which are non-separable in the original space into homogeneous groups in the high-dimensional space.
Sensor placement method for dynamic response reconstruction [29]	Wang, Law & Yang, 2014	Initial sensor combination is obtained by singular value decomposition of a re-assembled system Markov parameter matrix corresponding to all candidate sensor locations. A measurement noise effect index is defined and the final sensor placement is obtained by minimization of this index.	Numerical modelling: Plane truss structure and three-dimensional frame structure Sensors selected would lead to acceptable error of response reconstruction even with 5% measurement noise	A heuristic forward sequential sensor placement algorithm is used for minimization of the noise effect index
Optimal multi-type sensor placement for response and excitation reconstruction [32]	Zhang & Xu, 2015	An algorithm based on the framework of Kalman filter with unknown excitation is developed for the purpose.	Experimental and numerical testing: Simply supported overhanging steel beam. The method is independent of the type and time evolution of external excitation.	Reconstruction is done by extending the simultaneous input and state estimation of a linear stochastic system.

Table 2.2 Continued

Title	Authors	Approach	Testing and conclusions	Other notable points
A strain measurement model using a limited number of sensors for steel beam structures subjected to uncertain loadings [22]	Oh et al., 2015	A general form equation is determined from limited sensor data for strain measurement. To determine its coefficients an error function is developed. The partial derivative of this function with respect to each of the unknown coefficients provides a set of equations from which they can be derived. The optimal number of sensors required can also be obtained from the above process.	Experimental testing: Static loading on single- and multi-span beam structures. For the multi span beam with limited sensors large errors were observed.	Estimations of strain distributions are influenced by loading condition, order of approximation function and number and location of sensors.

2.3 Structural control strategies

In addition to response reconstruction, structural control can also be achieved using a damping system/device coupled with the right selection and placement of sensors. Control systems can limit the modal characteristics embedded in the response, be altered by structural deterioration and also play a role in redressing the design issues in a sensor network. Table 2.3, given at the end of this section provides a summary of some recent publications in this domain that are discussed here in detail.

Cazzulani, Resta, Ripamonti and Zanzi [7] have proposed a method based on Negative derivative feedback (NDF) for vibration control of flexible structures. The NDF compensator is a resonant control technique that works as a band-pass filter, cutting off control action far from the natural frequencies associated with the controlled modes and reducing spillover effect. Resonant control is a type of control logic, based on the modal approach, which calculates control action through a dynamic compensator to increase damping in a certain number of system modes. The NDF compensator shows better performance, both in terms of achieved damping and robustness to low and high frequency problems. Laflamme, Slotine and Connor [19] have developed a self-organizing input space for sequential adaptive control of structures. An innovative wavelet neural network (WNN) is adopted for the controller design and a self-organizing inputs algorithm (SOI) is developed for sequential input selection during control and identification of non-linear systems. The proposed system address the primary issues of limited measurements, uncertainties and immediate performance associated with controllers performing structural control of civil structures subjected to natural disasters.

A block diagram of the control system with the WNN-SOI controller is presented in Figure 2.2. The structure is subjected to forces from the excitation (y) and the control system (u). Both these parameters are fed under the input vector ζ to the proposed controller which gives an output neuro-controlled force u_n. This force is modified to u_{sl} by the sliding controller which in turn determines the voltage v in the control device that governs the control force u applied on the structure thus completing the loop. The method has been tested in a 39-story building in Boston and produced satisfactory results.

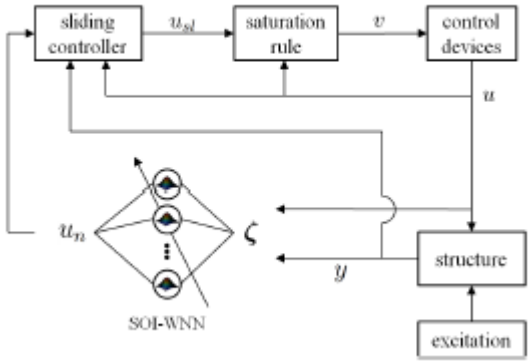

Figure 2.2 The closed loop control system [19]

Pnevmatikos and Thomos, [28] have studied stochastic structural control under earthquake excitations by investigating a control algorithm while considering the effects of structural deterioration. The algorithm remains constant while mass and stiffness are taken as random variables with the structural response being determined using Monte Carlo methods with and without employing control by a modified pole placement algorithm. It was found that variation of mass affects the controlled response while

variation of stiffness has negligible effect. Coefficient of variance of the displacement, velocity, and control force are in the range of 0.25-0.42 for the controlled analysis. Based on the results, the authors recommend that an analysis involving variation of mass should precede the installation of a control system and that the ratio of characteristic to deterministic value in control force should be calculated.

Apart from control algorithms and input selection methods, there are also a number of developments in damping control devices that can be placed along with the sensors in a structure. Bonello, Rafique and Shuttleworth, [6] have done the theoretical study of a smart electromechanical tuned mass damper beam device. A piezoelectric vibration energy harvesting (PVEH) beam is proposed as a tuned mass damper (TMD) which suppresses a particular vibration mode of the host structure over a broad band of excitation frequencies. This device is comprised of a pair of bimorphs shunted by a resistor–capacitor–inductor circuitry. Ideal degree of vibration attenuation can be achieved through appropriate tuning of the circuitry using an electromechanical TMD beam whose effective mass is less than 2% of the equivalent mass of the host structure at the targeted mode. In more recent research, Gonzalez-Buelga et al., [11] have developed an electromagnetic vibration absorber (EVA) with harvesting and tuning capabilities. An electromagnetic vibration transducer is connected as a resistance emulator across the motor terminals. This behaves mechanically as a damper, but is able to harvest the dissipated energy (in the resister) via the emulator. A voltage compensation unit is also designed to compensate for the coil losses. Results show that the maximum displacement of the host structure can be reduced by 20% when compared to a passive

control system further; the power needed to compensate for the losses in the coil is lower than the power available to harvest. The device is also capable of shifting its resonance in the mechanical domain, at a minimal energy cost, by connecting a capacitor or an inductor in parallel with the resistance emulator. Possible applications include systems presenting high flexibility. Gur, Roy and Mishra, [14] have proposed a Tuned liquid column ball damper (TLCBD) for seismic vibration control. TLCBD is a passive control device developed as an improvement of the Tuned liquid column damper (TLCD). A TLCD consists of a U-shaped tube filled with liquid (preferably water). Unlike TLCD, the TLCBD has a movable orifice modulating flow in the liquid column to improve the response reduction capability of the damper. The device is found to show better performance over TLCD for controlling stochastic vibration of structures while its performance is dictated by the optimum tuning ratio and the ball-to-tube diameter ratio.

Sun et al. [33] have established a benchmark problem in active structural control with wireless sensor network. A benchmark structure installed with Active Mass Driver (AMD) and developed in Simulink is instrumented with a wireless sensor network simulated using TOSSIM a state-of-the-art open-source simulator. Wireless signal and noise traces collected from a real-world multistory building are used as inputs to TOSSIM to realistically simulate the WSN. A sample optimal time-delay (OTD) controller is also provided with this benchmark. Wireless control design issues such as network-induced delay, data loss, available sensor measurements, measurement noises, and control constraints can be studied with this benchmark model.

Table 2.3 Summary of structural control strategies

Title	Authors	Approach	Testing and conclusions	Other notable points
Negative derivative feedback (NDF) for vibration control of flexible structures [7]	Cazzulani , Resta, Ripamonti & Zanzi, 2012	Works as a band-pass filter, cutting off control action far from the natural frequencies associated with the controlled modes and reducing spillover effect.	Experimental Testing: Clamped Aluminum beam. Shows better performance, both in terms of achieved damping and robustness to low- and high-frequency problems.	Resonant control is a type of control logic, whose objective is to increase damping in a certain number of system modes.
Self-organizing input space for control of structures. [17]	Laflamme, Slotine & Connor, 2012	An innovative neural network is developed with an adaptive input space for sequential input selection during control and identification of non-linear systems.	Experimental Testing: 39 story tower in Boston. Similar performance as a Linear Quadratic Regulator (LQR) for near field earthquakes and wind loads	It uses limited observations and can be adopted to non-stationarities.
A theoretical study of a smart electromechanical tuned mass damper beam device [6]	Bonello, Rafique & Shuttleworth, 2012	A piezoelectric vibration energy harvesting (PVEH) beam is proposed as a tuned mass damper (TMD) which suppresses a particular vibration mode of the host structure.	Ideal degree of vibration attenuation can be achieved through appropriate tuning of the circuitry using an electromechanical TMD beam whose effective mass is less than 2% of the equivalent mass of the host structure at the targeted mode.	This device is comprised of a pair of bimorphs shunted by resistor–capacitor–inductor circuitry. The optimal damping required by this TMD was generated by the PVEH effect of the bimorphs.

Table 2.3 Continued

Title	Authors	Approach	Testing and conclusions	Other notable points
Stochastic structural control under earthquake excitations [28]	Pnevmatikos & Thomos, 2014	A control algorithm is investigated considering effects of structural deterioration. The algorithm remains constant while mass and stiffness are taken as random variables and structural response under dynamic loads is determined with and without employing control	Numerical testing: Simulink models of single, three and eight-degree-of-freedom building systems. Variation of mass affects the controlled response while variation of stiffness has negligible effect.	Recommendation: An analysis involving variation of mass should precede the installation of a control system and the ratio of characteristic to deterministic value in control force should be calculated.
An electromagnetic vibration absorber (EVA) with harvesting and tuning capabilities [11]	Gonzalez-Buelga et al., 2015	An electromagnetic vibration transducer is connected as a resistance emulator across the motor terminals. This behaves mechanically as a damper, but is able to harvest the dissipated energy (in the resister) via the emulator. A voltage compensation unit was designed to compensate for the coil losses	Maximum displacement of the host structure can be reduced by 20% when compared to a passive control system. Possible application in systems presenting high flexibility.	The device can shift its resonance in the mechanical domain, at minimal energy cost, by connecting a capacitor or an inductor in parallel with the resistance emulator.
Tuned liquid column ball damper (TLCBD) for seismic vibration control [14]	Gur, Roy & Mishra, 2015	TLCBD is a passive control device developed as an improvement of the Tuned liquid column damper (TLCD). Unlike TLCD it has a movable orifice modulating flow in the liquid column to improve the capability of the damper.	Numerical testing: Single degree of freedom system subjected to deterministic ground accelerations recorded from real earthquakes. Better performance over TLCD for controlling stochastic vibration of structures.	TLCD consists of a U-shaped tube filled with liquid (preferably water). TLCBD's performance depends on the optimum tuning ratio and the ball-to-tube diameter ratio.

Table 2.3 Continued

Title	Authors	Approach	Testing and conclusions	Other notable points
Benchmark problem in active structural control with wireless sensor network [33]	Sun et al., 2015	A benchmark structure installed with Active Mass Driver (AMD) is developed in Simulink. The structure is instrumented with a wireless sensor network simulated using TOSSIM, a state-of-the-art open-source simulator. Delayed measurements that incorporate realistic data loss are used for closed-loop feedback control	Benchmark structure is a scaled model of a three-story building. Wireless control design issues such as network-induced delay, data loss, available sensor measurements, measurement noises, and control constraints can be studied with this benchmark model.	Wireless signal and noise traces collected from a real-world multistoried building are used as inputs to TOSSIM to realistically simulate the WSN. A sample optimal time-delay (OTD) controller is also provided with this benchmark.

3. MATHEMATICAL FORMULATION

3.1 Time Domain Decomposition method

The Time Domain Decomposition (TDD) technique uses mathematical concepts from the theory of linear algebra to decompose the structural response into its modal components. For this formulation, the multi-storied building can be envisioned as a long cantilever beam with *p* sensor positions. The structure's displacement response $y(t)$ is then a $p \times 1$ vector expressed in terms of the modal parameters as

$$y(t) = \sum_{i=1}^{\infty} c_i(t)\varphi_i \tag{3.1}$$

where, displacement $y(t) = [y_1(t), y_2(t).....y_p(t)]^T$, i^{th} mode shape $\varphi_i = [\varphi_{1i}, \varphi_{2i}.....\varphi_{pi}]^T$ and i^{th} modal contribution factor $c_i(t)$ is a scalar value. Considering that the continuous displacement response is sampled at a rate of *F* samples per second and assuming that *n* dominant and well separated modes can be resolved from this response within the folding frequency ($F_f = F/2$), Eq (3.1) can be modified as

$$y(t) = \sum_{i=1}^{n} c_i(t)\varphi_i + \varepsilon_t(t) \tag{3.2}$$

Since the number of sensors is finite, the second term is taken as the truncation error which indicates loss of information from higher modes.

$$\varepsilon_t(t) = \sum_{i=n+1}^{\infty} c_i(t)\varphi_i \tag{3.3}$$

In order to obtain mode isolated signals from the displacement response, 8th order Butterworth digital band pass filters designed separately for each of the visually identifiable frequency bandwidths are used. These digital filters can directly generate single degree of freedom time histories from the measured multi degree of freedom response; it must be noted here that the contribution of the truncation error (in Eq (3.3)) is insignificant as the band-pass filter weighs its pass band to unity and the other frequency components to zero. The i^{th} filtered single degree of freedom response at any time h is given as,

$$y_i(h) = c_i(h)\varphi_i + \varepsilon_f(h) \tag{3.4}$$

where, $y_i(h)$, $\varepsilon_f(h)$ and φ_i are $p \times 1$ vectors and $\varepsilon_f(h)$ represents noise due to both band pass filtering and residuals of $\varepsilon_t(h)$ (noise in Eq (3.3)). The noise vector can be spanned by its basis at the time sample h using the noise modes. Since $y_i(h)$ contains the modal space and the orthogonal noise space and the dimension of modal space being only one (the i^{th} mode shape vector), the dimension of the noise space amounts to $p-1$. Hence the noise vector is represented as,

$$\varepsilon_f(h) = \sum_{j=1}^{p-1} d_j(h)\psi_j \tag{3.5}$$

where, the $p \times 1$ vector, $\psi_j = [\psi_{1j}, \psi_{2j} \ldots\ldots\ldots \psi_{pj}]^T$ represents the j^{th} orthogonal noise bases and the scalar $d_j(h)$ represents the contribution of the j^{th} noise mode to the total noise vector at the sample time h. Then substituting Eq (3.5) into Eq (3.4), the mode-isolated displacement vector is written as

$$y_i(h) = c_i(h)\varphi_i + \sum_{j=1}^{p-1} d_j(h)\psi_j \tag{3.6}$$

Considering that a total of *N* samples are measured at each of the *p* locations, the matrix form of Eq (3.6) becomes

$$\begin{bmatrix} y_{1i}(1)\dots y_{1i}(N) \\ \vdots \quad \ddots \quad \vdots \\ y_{pi}(1)\dots y_{pi}(N) \end{bmatrix} = \begin{bmatrix} \varphi_{1i} \\ \vdots \\ \varphi_{pi} \end{bmatrix} [c_i(1)\cdots c_i(N)] + \sum_{j=1}^{p-1} \begin{bmatrix} \psi_{1i} \\ \vdots \\ \psi_{pi} \end{bmatrix} [d_j(1)\cdots d_j(N)] \tag{3.7}$$

This can be written in a simplified manner as

$$Y_i = \varphi_i c_i^T + \sum_{j=1}^{p-1} \psi_j d_j^T \tag{3.8}$$

where the $p \times N$ matrix, Y_i, represents the mode-isolated output time history that contains only the i^{th} mode. The $N \times 1$ vector $c_i = [c_i(1)\cdots c_i(N)]^T$, denotes the i^{th} modal contribution of the displacement response and the $N \times 1$ vector $d_j = [d_j(1)\dots d_j(N)]^T$, denotes the j^{th} noise contribution.

A cross-correlation E_i of the i^{th} mode-isolated time history signals is now developed. The $p \times p$ matrix E_i, can be interpreted as the energy correlation matrix of the i^{th} mode with respect to the location of sensors.

$$E_i \equiv Y_i Y_i^T \tag{3.9}$$

Substituting Y_i from Eq (3.8) into Eq (3.9),

$$E_i = \varphi_i c_i{}^T c_i \varphi_i{}^T + \varphi_i c_i{}^T \sum_{j=1}^{p-1} d_j \psi_j{}^T + \sum_{j=1}^{p-1} \psi_j d_j{}^T c_i \varphi_i{}^T + \sum_{j=1}^{p-1}\sum_{k=1}^{p-1} \psi_j d_j{}^T d_k \psi_k{}^T \tag{3.10}$$

Now, the orthogonal bases in Eq (3.10) can be simplified based on the orthogonality property, hence,

$$c_m^T c_n = \begin{cases} q_m, & m = n \\ 0, & m \neq n \end{cases} \qquad d_m^T d_n = \begin{cases} \sigma_m, & m = n \\ 0, & m \neq n \end{cases} \text{ and } \; c_m^T d_n = d_m^T c_n = 0 \tag{3.11}$$

Thus Eq (3.10) can be written as,

$$E_i = \varphi_i q_i \varphi_i^T + \sum_{j=1}^{p-1} \psi_j \sigma_j \psi_j^T \tag{3.12}$$

where the physical representation of the scalar values, $q_i = c_i^T c_i$ and $\sigma_j = d_j^T d_j$ (at m=n) is the level of energy at the modes i and j respectively. Eq (3.12) can be re-written as

$$E_i = U \Omega U^T \tag{3.13}$$

where $U \equiv \left[\varphi_i \; \psi_1 \cdots \psi_{p-1} \right]$ is the $p \times p$ singular vector matrix of Y_i and $\Omega \equiv diag\left[q_i \; \sigma_i \cdots \sigma_{p-1} \right]$ is the $p \times p$ singular value matrix of Y_i and it is assumed that $q_i > \sigma_1 > \cdots > \sigma_{p-1}$. Therefore, the required i^{th} un-damped mode shape φ_i can be obtained by taking the first singular vector after the singular value decomposition (SVD) of the correlation matrix E_i.

3.2 Allied results

The mode shapes obtained from the above process are in turn used to generate the modal contribution factors from which the modal frequencies, damping ratios and finally the reconstructed responses are derived. To obtain the modal contribution factor c_i, Eq (3.8) is pre-multiplied by the transpose of the i^{th} mode shape vector φ_i

$$\varphi_i^T Y_i = \varphi_i^T \varphi_i c_i^T + \varphi_i^T \sum_{j=1}^{p-1} \psi_j d_j^T \tag{3.14}$$

Since the noise bases are orthogonal to the modal bases, the second term on the right hand side of Eq (3.14) can be eliminated, hence the modal contribution factor is given as

$$c_i^T = \frac{1}{\varphi_i^T \varphi_i} \varphi_i^T Y_i \tag{3.15}$$

This signal represents the i^{th} modal behavior of the input displacement response for the entire set of p signals. Thus, its auto-spectrum produces a single peak (Figure 3.1) whose frequency f_i is the damped natural frequency of the i^{th} mode. The modal damping ratio is then derived using the half power bandwidth method. Frequencies f_{1i} and f_{2i} corresponding to $1/\sqrt{2}$ of the peak amplitude A are located in the graph, and the damping ratio ζ_i is given as

$$\zeta_i = \frac{f_{2i} - f_{1i}}{2 f_i} \tag{3.16}$$

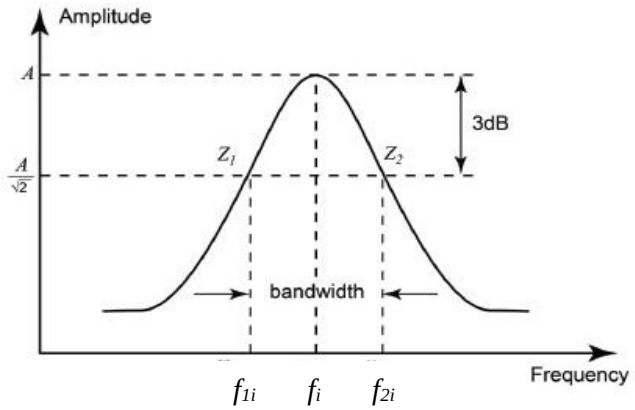

Figure 3.1 Half power bandwidth method illustration [10]

The equation for response reconstruction is given as

$$y = \varphi^T c \tag{3.17}$$

where φ is an $n \times p$ matrix of mode shapes, c is an $n \times N$ matrix of modal contribution factors and y is the $p \times N$ matrix of reconstructed responses. Its accuracy thus depends on the number of modes identified (*n*), number of sensors considered (*p*) and the accuracy of filtered responses considered in the derivation of the modal contribution factors.

4. PRELIMINARY STUDIES: 20-STORY BUILDING

The objective of this research study is to determine the applicability of Time Domain Decomposition (TDD) method under the context of dynamic response from multi storied buildings. Since, TDD methodology has not been used to study the multi-hazard excitation of tall buildings, it is of interest to first establish the level of accuracy obtainable from this approach when compared with finite element results. For this purpose, only seismic responses are considered as seismic time histories are readily available and are easy to analyze with the built in tools in modern finite element packages.

4.1 Model description

A 20-story Los Angles structure designed as part of the SAC Steel Project [13] is adopted for this analysis. Its selection is primarily due to the availability of complete design and loading details as well as its location in a high seismicity area that makes it an ideal candidate for seismic analysis. The building is predominantly a steel structure with composite concrete floor slabs. The structural system consists of exterior moment resisting frames with moment resisting connections and box columns at its corners to resist bi-axial bending. All columns are designed to bend about the strong axis. The structure also has two floors below ground whose beam-column joints are specified to have pinned connections. Similarly end conditions are also taken to be pinned. A centerline model is deemed sufficient for this analysis as the dynamic properties do not show much change on incorporating more features such as modelling the panel zones

and considering the clear span of structural elements (rather than the centerline distance). This is because the decrease in stiffness due to modelling of panel zones is nearly compensated by the increase in stiffness due to reduced length of structural elements [13]. Finite element software SAP 2000 [30] is chosen to model the structure as it provides a wide variety of tools to analyze dynamic loads. Figure 4.1 shows the building's computational model and geometric dimensions.

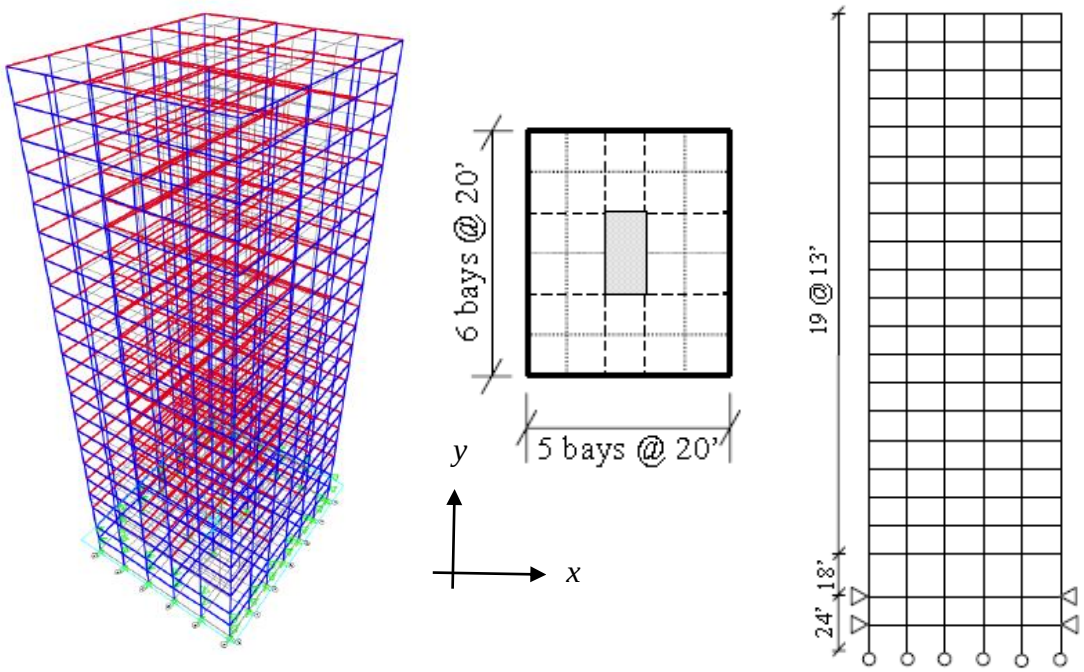

(a) **(b)**

Figure 4.1 20-story building a) Finite element model b) Geometric dimensions [13]

The assigned dead loads are considered as the mass source for the structure while the frame and slab sections provide the necessary stiffness. A uniform damping of 1.5%

is specified for all modes and the rigid diaphragm constraint is incorporated to ensure that each floor slab behaves as a single entity within its plane. Results of the modal analysis are as shown in Table 4.1. The first 12 modes are grouped together based on their specific translational and torsional nature.

Table 4.1 Time periods in seconds of the first 12 modes

Sno.	Translational 1 (XZ) Plane	Translational 2 (YZ) plane	Torsional
1.	3.93	3.57	2.38
2.	1.38	1.26	0.85
3.	0.81	0.75	0.5
4.	0.57	0.53	
5.	0.43		

4.2 Seismic loading and analysis

Since the building is representative of a Los Angles structure, two sets of historical seismic time histories recorded in parts of California are selected ([3], [32]). The selected ground motions correspond to recordings of crustal earthquakes with a 10% probability of exceedance in 50 years. Each set consists of two recordings for the same seismic event corresponding to the fault normal (fn) and fault parallel (fp) directions. Their characteristics are briefly summarized in Table 4.2. For ease of representation, an abbreviated version of the names of the seismic loadings are used in further sections. The abbreviation has three parts; the seismic event (iv for Imperial Valley or nr for Northridge), its component (n for fault normal or p for fault parallel) and the direction of application (x for along X axis, y for along Y axis or rz for being about the rotational Z

axis). Hence each time history has three abbreviations for each direction of application. For example ivnx can be expanded as Imperial Valley fault normal earthquake applied along the X axis.

Table 4.2 Characteristics of selected ground motions ([3], [32])

Earthquake Record	Abbreviations	Magnitude	Scale factor	Peak Ground Acceleration (in/s^2)	Duration (s)
Imperial Valley, 1940, El Centro (fn)	ivnx, ivny, ivnrz	6.9	2.01	177.96	39.38
Imperial Valley, 1940, El Centro (fp)	ivpx, ivpy, ivprz	6.9	2.01	260.98	39.38
Northridge, 1994, Rinaldi RS (fn)	nrnx, nrny, nrnrz	6.7	0.79	206.02	14.95
Northridge, 1994, Rinaldi RS (fp)	nrpx, nrpy, nrprz	6.7	0.79	223.85	14.95

Time histories of the above excitations are shown in Figure 4.2 below. The Imperial Valley recording has a sampling frequency of 50Hz while the Northridge recording has a sampling frequency of 200Hz making the former a much longer time history [3]. It is observed that the fault-normal and fault-parallel components of each set exhibit similar behavior in terms of occurrence of peaks and general profile of excitation. Both earthquakes appear to display a nearly constant mean of zero.

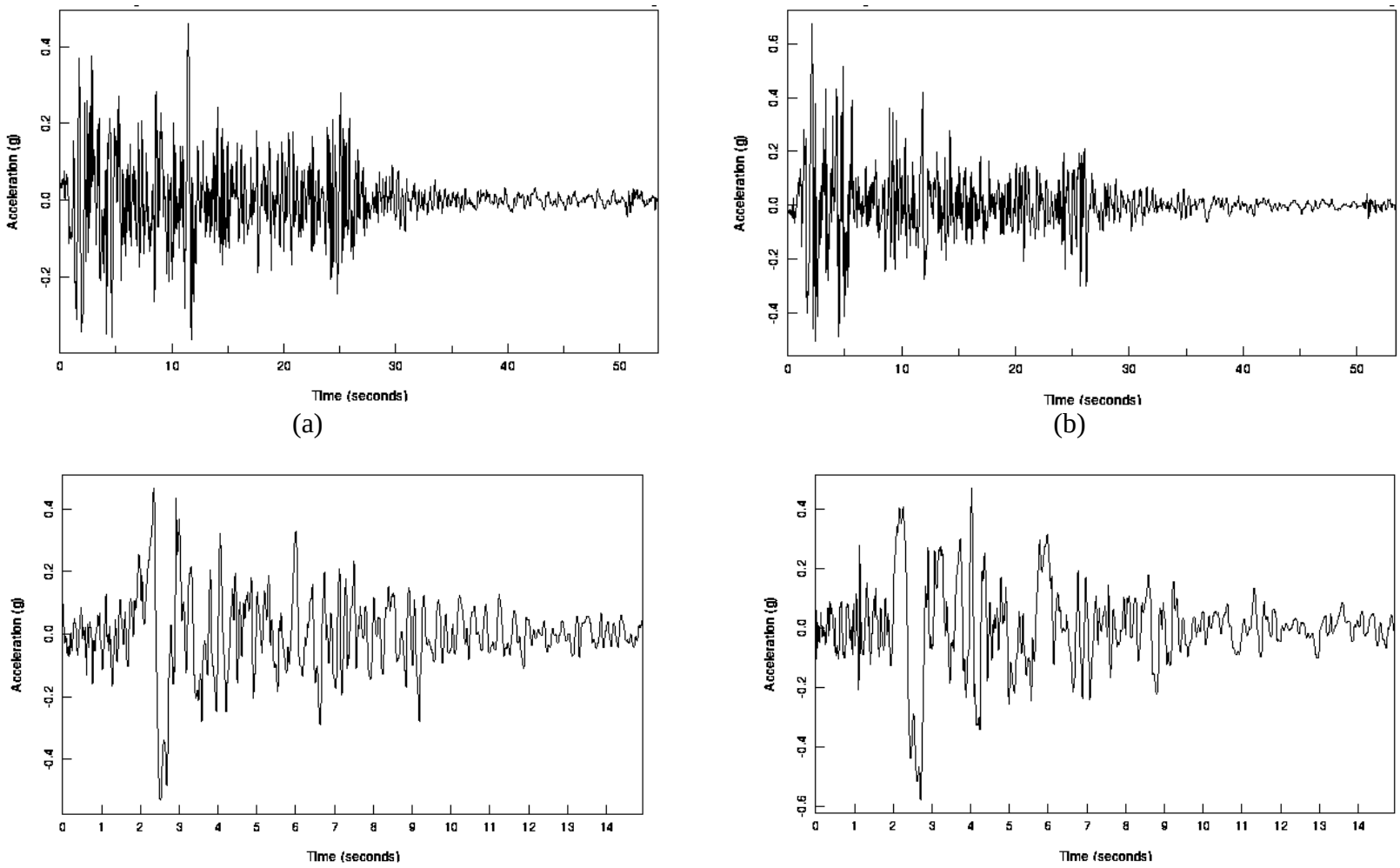

Figure 4.2 Input excitations a) Imperial Valley (fn) b) Imperial Valley (fp) c) Northridge (fn) d) Northridge (fp) [3]

A linear time history analysis was carried out using SAP 2000 [30] by applying each of these excitations successively first along the X-axis (ivnx, ivpx, nrnx and nrpx), then the Y-axis (ivny, ivpy, nrny and nrpy) and about the rotational Z axis (ivnrz, ivprz, nrnrz and nrprz). The resulting displacements are recorded in the direction of loading leading to a total of sixteen response cases -four along the X-axis, four along the Y-axis and four about the rotational Z-axis. The method of application is chosen in the above manner in order to maximize the magnitude of responses obtained.

For the purpose of the TDD analysis, it is assumed that one sensor is located at the same position in every floor of the 20-story building. Each sensor captures responses at 20,000 time steps for a single input excitation. The sampling frequency is taken to be the same as that of the loading for the Northridge responses leading to a total response time of 100s while it is taken as 100 Hz for the Imperial Valley case thus capturing the response for 200s. The responses along the X and Y axis are used to obtain the first three translational modal characteristics along the XZ and YZ planes respectively while those along the rotational Z axis are used in deriving the first three torsional modal characteristics. Hence on comparing with the notation used in Chapter 3, for this analysis $n=3$, $p=20$ and $N=20,000$. A detailed discussion of the modal results is covered in the sections below.

4.3 Translational modal characteristics

Power spectral densities of the X and Y directional displacements obtained from the sensors located in the 20th floor are presented in succession in Figures 4.3 and 4.4.

The graphs illustrate the contribution of each modal frequency towards the input response.

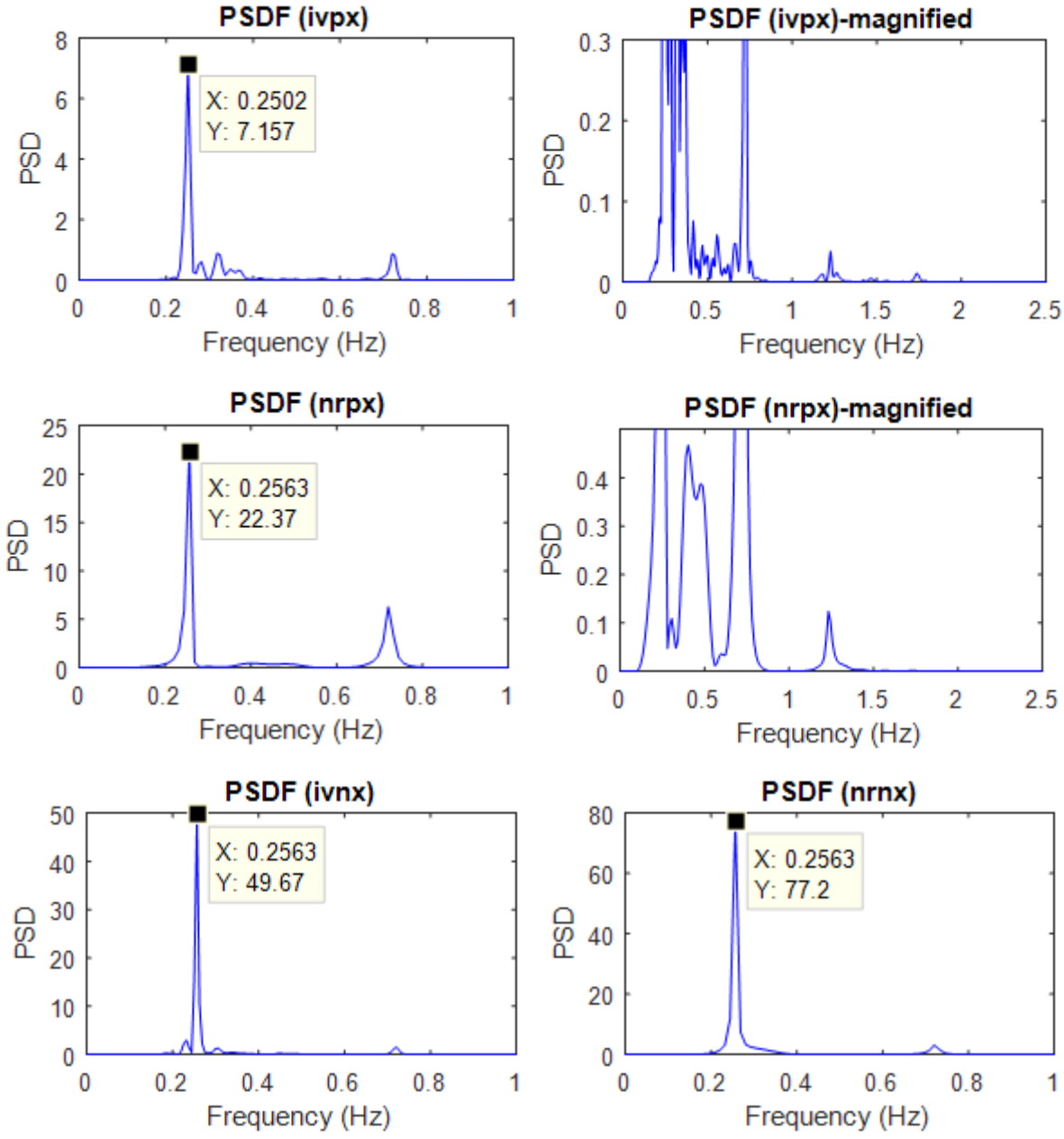

Figure 4.3 Power spectral density functions of displacements along the X axis

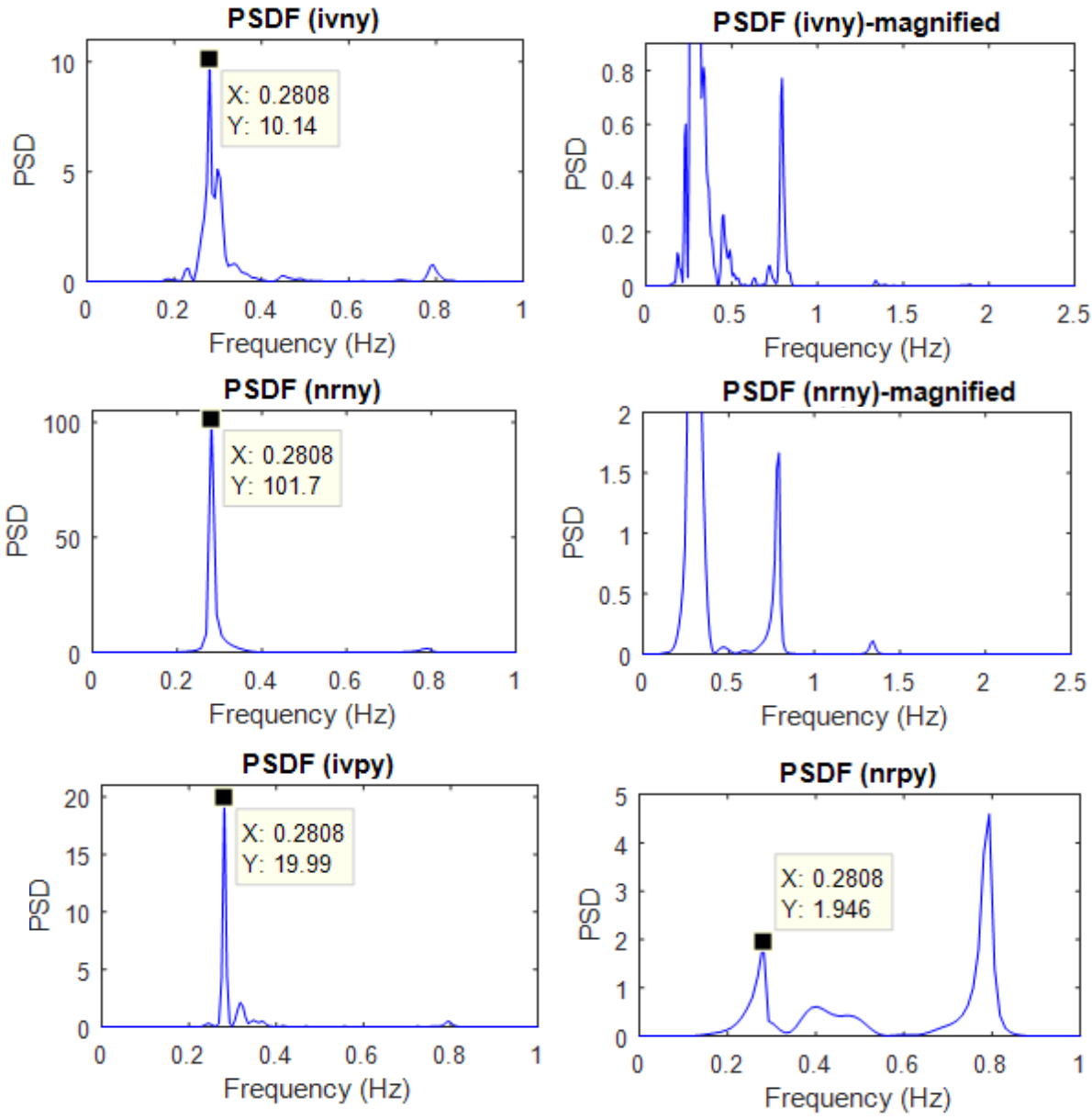

Figure 4.4 Power spectral density functions of displacements along the Y axis

As anticipated, responses along the X direction display the XZ modal frequencies and those along the Y direction represent the YZ modal frequencies. In all cases except one (nrpy), power of the first mode is much larger than that of all other modes. The

magnified graphs show that there is negligible contribution beyond the first three modes. The identified frequencies are used to design band pass filters used in the TDD process to ultimately derive the structure's inherent mode shapes represented in Figures 4.5 to 4.7 below.

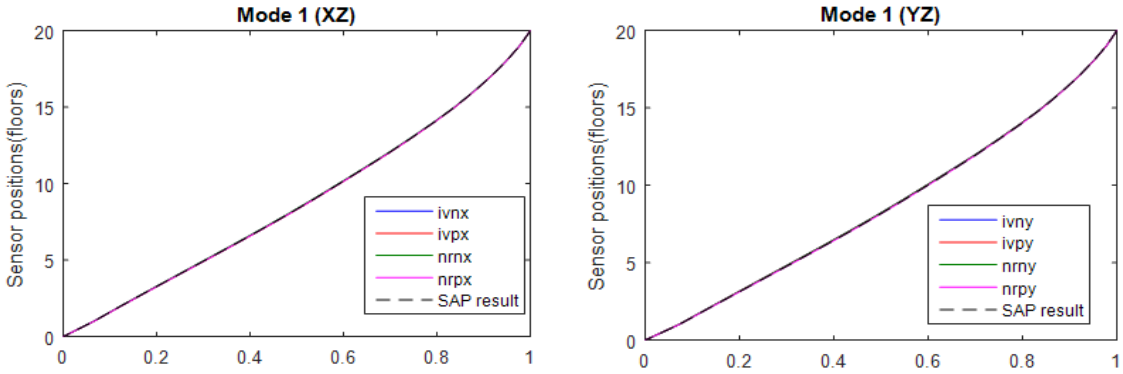

Figure 4.5 First translational mode shape along the XZ and YZ planes

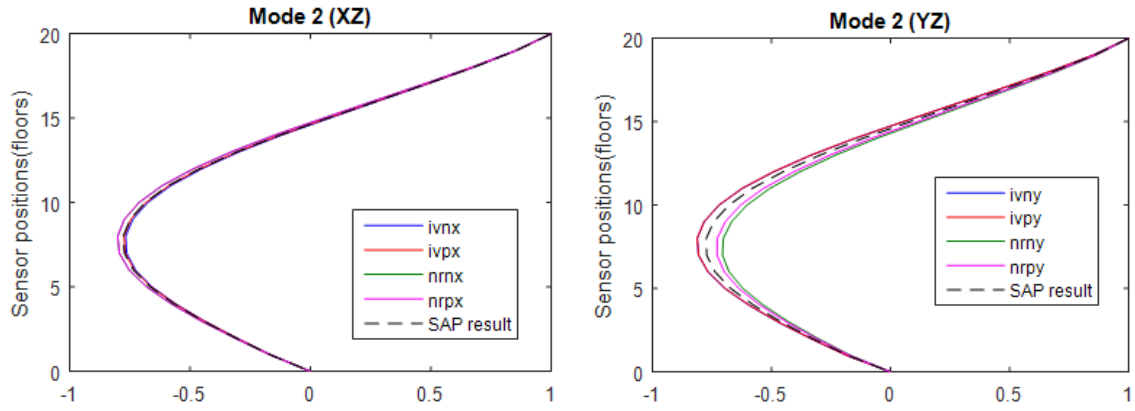

Figure 4.6 Second translational mode shape along the XZ and YZ planes

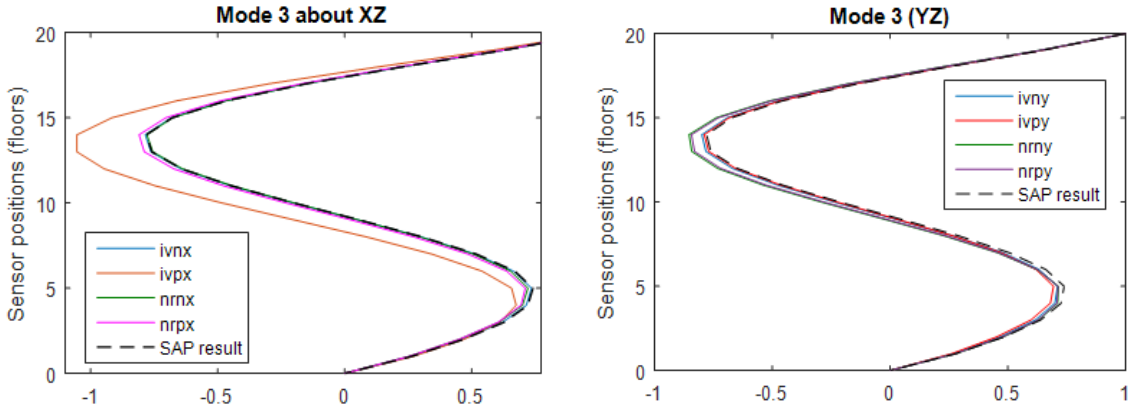

Figure 4.7 Third translational mode shape along the XZ and YZ planes

Negligible errors are observed in most cases. The third mode shape derived from the ivpx response appears as the only outlier in the group. Maximum variation occurs between the 10^{th} – 16^{th} floors producing an error of about 35%. Modal time periods and damping ratios are given in Tables 4.3 and 4.4 respectively.

Table 4.3 Translational modal periods in seconds

Ground Motion	Time Periods (XZ)			Time Periods (YZ)		
	Mode 1	Mode 2	Mode 3	Mode 1	Mode 2	Mode 3
Imperial Valley, (fn)	3.90	1.39	0.81	3.56	1.26	0.75
Imperial Valley, (fp)	4.00	1.39	0.82	3.56	1.26	0.75
Northridge, (fn)	3.90	1.39	0.81	3.56	1.26	0.75
Northridge, (fp)	3.90	1.39	0.81	3.56	1.26	0.75
SAP result	3.93	1.38	0.81	3.57	1.26	0.75

Table 4.4 Translational modal damping ratios

Ground Motion	% Damping ratios (XZ)			% Damping ratios (YZ)		
	Mode 1	**Mode 2**	**Mode 3**	**Mode 1**	**Mode 2**	**Mode 3**
Imperial Valley, (fn)	0.95	0.76	0.67	1.07	0.98	0.51
Imperial Valley, (fp)	1.54	0.63	0.64	0.8	0.78	0.68
Northridge, (fn)	1.57	1.08	0.86	1.45	1.38	0.99
Northridge, (fp)	1.64	1.08	0.98	2.29	1.11	1.05
SAP result	1.5	1.5	1.5	1.5	1.5	1.5

The modal time periods appear to display excellent similarity with the finite element results. The modal damping ratios on the other hand display a range of values from 2.29-0.51% while the finite element model was given a constant damping ratio of 1.5%. On close observation, it appears that although there is a significant dip between the first and second modal ratios, the difference is comparatively smaller between the second and third modes suggesting that the ratios may tend to become constant with higher modes.

4.4 Torsional modal characteristics

The torsional mode shapes are given in Figure 4.8 and the subsequent modal periods and damping ratios are presented in Table 4.5.

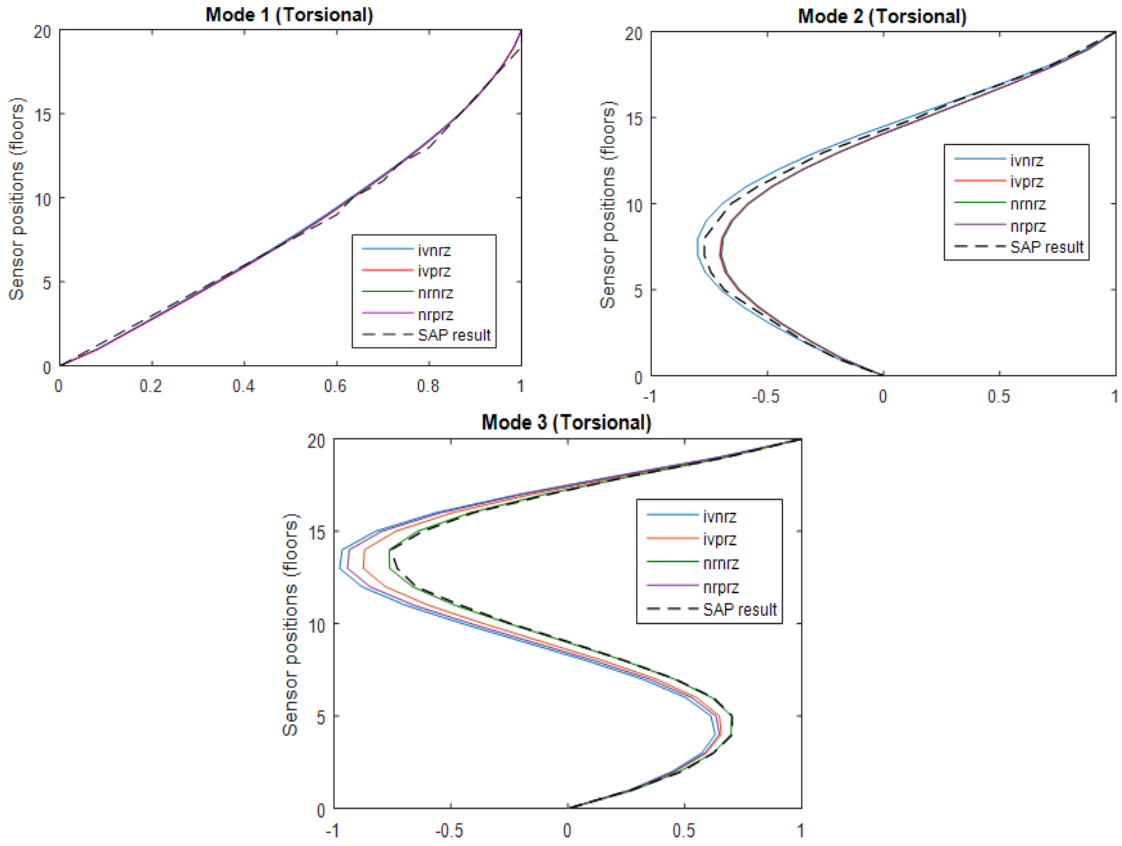

Figure 4.8 Torsional mode shapes

Table 4.5 Torsional modal frequencies and damping ratios

Ground Motion	Modal Periods			% Damping ratios		
	Mode 1	Mode 2	Mode 3	Mode 1	Mode 2	Mode 3
Imperial Valley, (fn)	2.24	0.84	0.51	1.34	0.89	0.49
Imperial Valley, (fp)	2.38	0.85	0.51	0.98	0.77	0.52
Northridge, (fn)	2.34	0.85	0.50	1.65	1.25	0.78
Northridge, (fp)	2.41	0.85	0.50	2.28	1.15	1.45
SAP result	2.38	0.85	0.50	1.50	1.50	1.50

With regards to the derived mode shapes, there is an increase in error with higher modes especially along the bends. The derived modal periods show some variation in the first mode however higher modal results are very satisfactory. The range of variation

in the percentage modal damping ratios is quite similar to the translational case. There appears to be a case where (nrprz) where there is an increase in the damping value from the previous mode.

4.5 Motivation for advanced analysis

All values reported in this chapter are derived from responses obtained along the direction of application of ground motion. The responses also have a high sampling frequency (a total of 20,000 samples per ground motion) and all 20 floors are considered to have a sensor recoding the translational and rotational displacements. This ensures that the modal characteristics are derived from large response matrices having the maximum magnitudes possible for this scenario. The resulting modal characteristics hence display significant similarly with the finite element results even for higher modes. The modal frequencies appear to produce nearly exact values and the mode shapes and damping ratios are within acceptable error limits.

However this analysis is not very representative of real world conditions where earthquakes are not the only prevalent dynamic loads, number of sensors are limited and response reconstruction of unknown floor level responses are required. In order to address these concerns, it is necessary to consider the action of wind loading on structures, limit the number of sensors and explore the possibility of sensor damage. To carry out such studies analyzing longer and slender structures whose responses can better capture the inherent modal characteristics under such scenarios is necessary. The subsequent chapters explore the options for considering an ideal prototype to depict this process and the resulting advanced analysis follows.

5. DYNAMICS OF TALL BUILDINGS

From the discussion of results in the previous chapter, the TDD methodology was shown to produce satisfactory results for 20-story buildings, however it is not obvious for taller buildings having a higher level of flexibility how this will affect the response reconstruction process. A better understanding of the dynamics of tall and super tall buildings is needed in order to develop a representative finite element model for the numerical simulations. Taller buildings also present the challenges of determining the optimized number and placement of sensors to ultimately achieve optimal reconstruction results.

5.1 Structural systems and material characteristics

Compared to a low-rising building, the requirements of strength, stability and serviceability are much higher for a tall structure. Hence, the dynamic behavior of high-rises is of greater importance and its governing features remain embedded within the structure's fundamental design. To understand this behavior, it is essential to look into the building's mass, stiffness and damping properties, all three of which are directly dependent on the chosen structural system and material composition. This choice is often difficult and is governed by a vast domain of features including the structure's height, slenderness, location, usage and architectural requirements such as aesthetics and shape. Technological advancements have also played a major role in the process, increasing the constructible height through new methodologies in design, construction and materials research. For instance, the development of self-climbing formwork has

encouraged the selection of concrete as the primary construction material over steel as observed in One World Trade Center (New York City, 2014) and Burj Khalifa (Dubai, 2008). A study of the 100 tallest buildings in the world shows that the use of steel as a structural material has fallen from being 90 % in the 1970s to a mere 17% in the present day, shifting to concrete and composite structures [27]. Figure 5.1 shows the structural materials used in some of the popular skyscrapers.

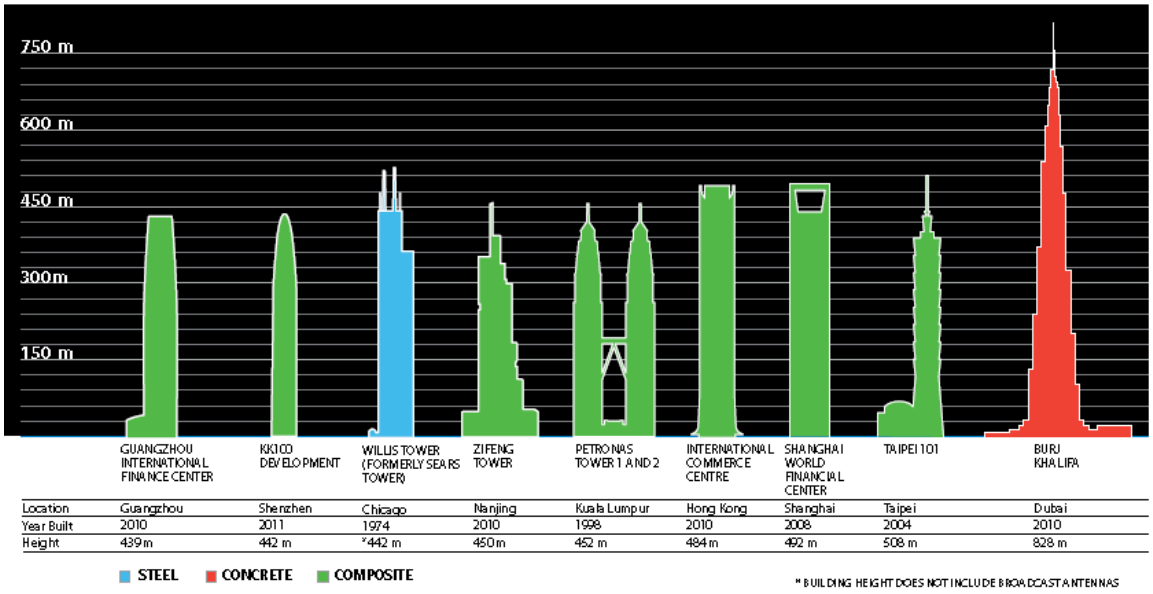

Figure 5.1 Primary structural materials used in the world's tallest buildings [27]

The governing dynamic load also plays an important role in material selection. Steel being more ductile and having less mass often results in lower seismic forces. It is also more dimensionally stable unlike concrete, which has to deal with effects of creep and shrinkage. High strength concrete on the other hand provides strength and stiffness economically and has greater inherent damping. Its properties make it an ideal material

for wind resistant design. Composite systems try to mix the advantages of both these materials. Recent practices have seen concrete vertical systems that can economically carry heavy compressive loads being used along with steel flooring systems that can provide long column less spans. Composite systems are also found in places subjected to extreme loading where external damping systems (Figure 5.2) have been placed to reduce their impact like the case of Taipei 101.

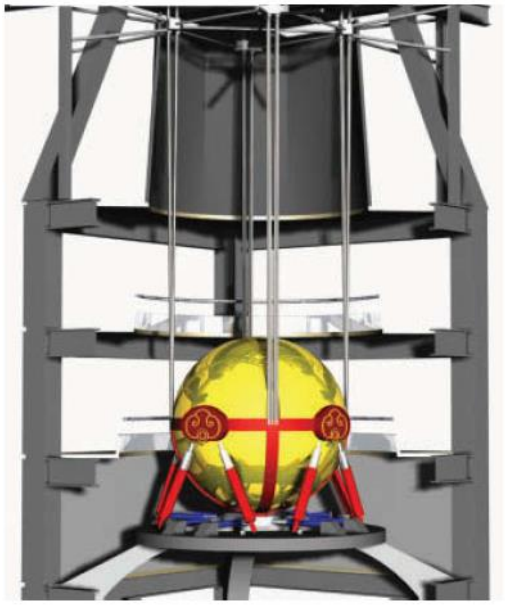

Figure 5.2 Passive tuned mass damper in Taipei 101 [27]

Structural systems are found to primarily impact the building's stiffness and differ their shear resisting capacity. A stiff shear system is necessary for the structure to act as a single huge cantilever beam rather than an aggregation of individual subsystems. For both steel and concrete systems, simple moment frames are sufficient for 20-30 story buildings with normal floor size. For taller structures, more closely spaced frames (tube

systems or tube-in tube systems) with lateral bracing and walls may be adopted. The configurations of these systems have changed through the years to have more taller, slender and aesthetically pleasing buildings. In the towers of 1960s and 70s, lateral systems were mostly found along the perimeter of the buildings. However having closely spaced columns and lateral bracings resulted in dense exteriors. The contemporary practices have implemented interior shear resisting systems. But this often results in a slender core for tall structures leading to excessive flexural deformations. In such cases, outriggers are provided transferring the overturning moment from the core to the external vertical elements. The Burj Khalifa with a concrete buttressed core is a good example for such a system. Figure 5.3 shows Fazlur Khan's classification of structural systems with regards to building heights.

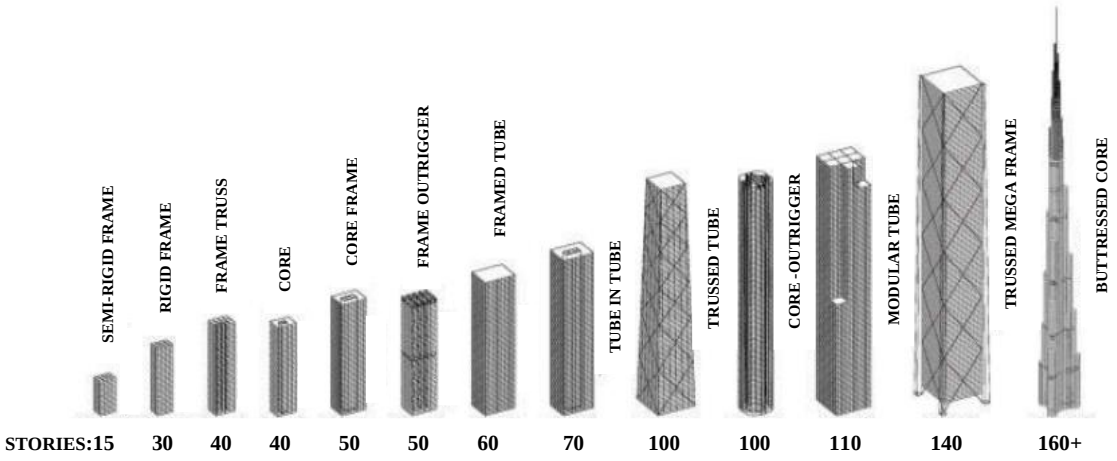

Figure 5.3 Tall building systems [27]

5.2 Estimation of fundamental periods

An estimation of the fundamental modal periods of a representative group of tall buildings from around the world is presented in this section (Table 5.1). Since the objective of this thesis is to emphasize on the instrumentation of aging infrastructure, the selected group covers more than a century of multi-storied construction while tracking the inherent advancement in building height. The estimation is done by means of a simple intuitional formula and a more advanced structural design code based provision as listed below.

Formula 1 [31]:

$$T_1 = \frac{Number\ of\ \ floors}{10} \tag{5.1}$$

Formula 2 as per ASCE/SEI 7-05 [5]:

$$T_2 = C_t h_n^x \tag{5.2}$$

where, h_n is height in ft above the base of the building and

$C_t = 0.028$, x=0.8 for steel moment resisting frames

$C_t = 0.016$, x=0.9 for concrete moment resisting frames

for composite frames, the average of both concrete and steel frames is taken.

Structures with simple (rectangular/square) and consistent cross sectional geometries are selected so that they are a good fit with the chosen formulae and provide nearly dependable results. A second table (Table 5.2) of modal periods estimated from field calculations or finite element analysis is also provided below Table 5.1.

Table 5.1 Approximate fundamental periods of some tall buildings

Structure	Location	Date completed	Floors above ground	Height (ft)[+]	Estimation with T_1 (s)	Estimation with T_2 (s)	Structural material
Taipei 101	Taipei, Taiwan	2004	101	1437	10.1	10.26	Composite
Petronas Twin Towers	Kuala Lumpur, Malaysia	1998	88	1230	8.8	8.98	Composite
Central Plaza	Hong Kong, China	1992	78	981	7.8	7.88	Concrete
One Canada Square	London, UK	1991	50	774	5	6.05	Composite
Bank of America Plaza	Dallas, USA	1985	72	921	7.2	7.02	Composite
Sunshine 60	Tokyo, Japan	1978	60	787	6	6.14	Composite
Willis Tower	Chicago, USA	1974	108	1451	10.8	9.47	Steel
Aon Center	Chicago, USA	1973	83	1136	8.3	7.79	Steel
One Shell Plaza	Houston, USA	1970	50	714	5.0	5.92	Concrete
555 California Street	San Francisco, USA	1969	52	779	5.2	5.76	Steel
Prudential Tower	Boston, USA	1964	52	750	5.2	5.59	Steel
Empire State Building	New York City, USA	1931	102	1250	10.2	8.41	Steel
Chrysler Building	New York City, USA	1930	77	828	7.7	6.05	Steel
Metropolitan Life Insurance Company Tower	New York City, USA	1909	50	700	5	5.29	Steel

[+]*Structural height without considering the length of antenna or spire wherever applicable (subject to availability of information). Source Council on Tall Buildings and Urban Habitat (CTBUH) [4]*

Table 5.2 Calculated time periods of some tall buildings

Structure	Location	Date completed	Floors above ground	Height (ft)[+]	Fundamental Time Period (s)		
					Mode 1 (Translational)	Mode 2 (Translational)	Mode 3 (Torsional)
Burj Khalifa [31]	Dubai, UAE	2010	163	2723	11	10	4
Jin Mao Tower [31]	Shanghai, China	1999	88	1380	5.7	5.7	2.5
Jinao Tower[31]	Nanjing, China	2013	56	759	5	4.8	3.6
John Hancock Center [36]	Chicago, USA	1969	100	1128	7	4.9	Not known

[+]*Structural height without considering the length of antenna or spire wherever applicable (subject to availability of information), source CTBUH [4].*

Table 5.2 is provided to get a relatively accurate representation of tall building behavior and provide a benchmark for the reliability of the previously estimated periods in Table 5.1. A pictorial representation of the first three modes of Burj Khalifa (as stated in Table 5.2) is shown in Figure 5.4.

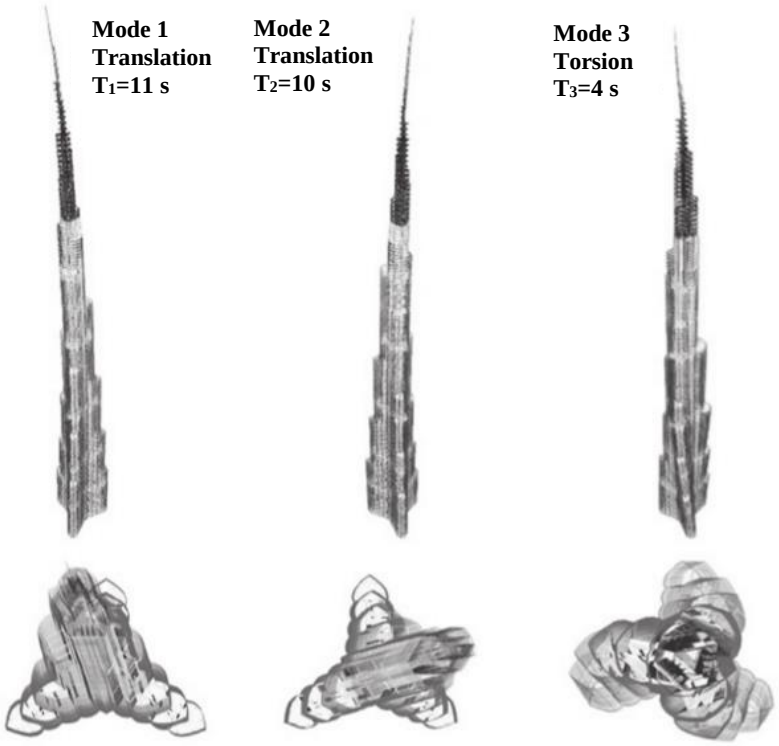

Figure 5.4 Modal frequencies of Burj Khalifa [31]

On comparing structures with considerable variation in height, slenderness is the governing feature distinguishing their flexibility. Hence, the tallest structure in the group should most likely be the one with the highest modal period. Considering that the Burj Khalifa has a calculated period of 11s (from Table 5.2), it can be fairly stated that

the approximation formulae employed in Table 5.1 are conservative since it should be around 16.3s when calculated with those methods. Also, the level of conservativeness appears to increase with building height. This is because the actual relationship between building height and fundamental period is not a simple linear one but has a complex dependence on several parameters as observed from the values in Table 5.2. Hence the notion that a 50-story steel building may have a fundamental period of about 5s may be more precise than stating that a 100-story building may have a period of 10s. In addition, the estimated results do not take into consideration the increased stiffness due to extreme loading. This can be seen from a comparison of the Jin Mao Tower and Taipei 101. Both these buildings are located in regions of high wind and earthquake loading and also have comparable heights. However, the calculated period of Jin Mao is virtually half of the estimated periods of Taipei 101.

Following the above discussion, the Prudential Tower, Boston is selected as the prototype for the finite element model. Being in Boston, it is likely that the tower may not be designed for very heavy earthquake loads. In addition, due to its relatively shorter height, the estimated periods could be more realistic in this case. It is also the oldest building of its kind in the list built with a steel tube in tube concept, which is simple to model. The much older Metropolitan Life Insurance Company tower was not selected as it belongs a much older period whose design practices may be hard to replicate without much more information.

6. NUMERICAL SIMULATIONS: 52-STORY BUILDING

Unlike the case of the 20-story building, the objective for these numerical simulations is to investigate other aspects of the TDD methodology. Thus, this Chapter is focused on investigating optimal sensor placement pattern in order to obtain accurate response reconstruction for cases involving various multi-hazard loading scenarios. Further, the numerical simulations address sensor failure during disasters and its impact on the reconstructed time series.

6.1 Model description

For the purpose of this analysis, a model resembling the dynamic properties of the Prudential Tower, Boston is simulated in SAP 2000 [30]. The model consists of 52 floors above ground and is primarily a steel structure with concrete floor slabs. The exterior moment resisting frames consist of closely spaced columns (10ft apart) resembling a tubular system to provide the necessary stiffness. The model has a uniform square cross section with a side of 150ft and a total structural height of 663ft. Other modelling and analysis assumptions are similar to the 20-story building as previously discussed in section 4.1. A centerline model is considered for this analysis with uniform modal damping of 1.5%. Figure 6.1 shows the Prudential Tower and a cross-section of the idealized finite element model.

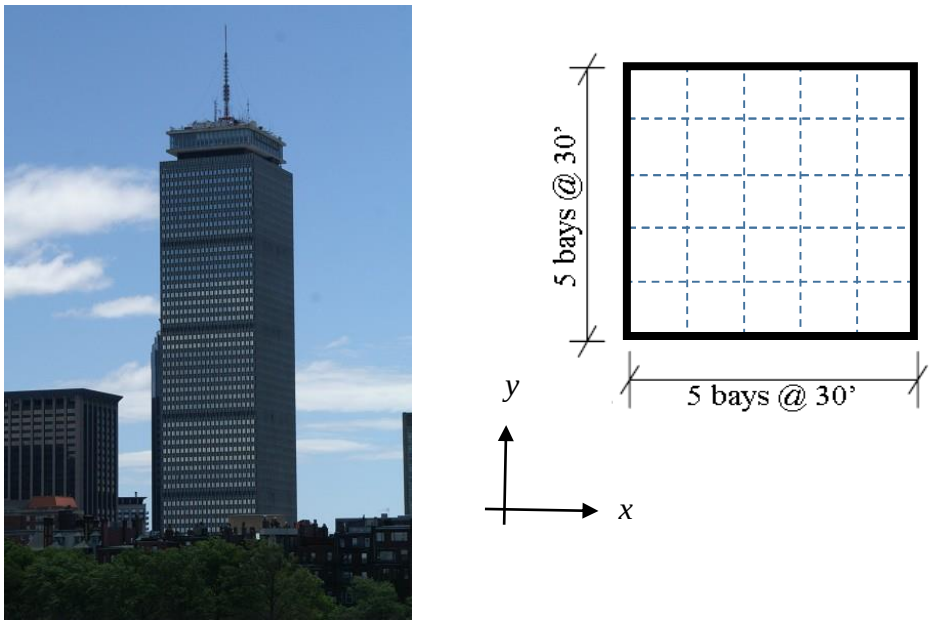

Figure 6.1 The Prudential Tower, Boston and a cross-section of its model [2]

Modal periods of the finite element prototype are as shown in Table 6.1. The first 15 modes are grouped together based on their specific translational and torsional nature. The results are in line with the data gathered in Chapter 5 regarding the expected modal periods of a building of such height.

Table 6.1 Time periods in seconds of the first 15 modes

Sno.	Translational 1 (XZ) Plane	Translational 2 (YZ) plane	Torsional
1.	4.19	5.73	3.42
2.	1.48	2.09	1.27
3.	0.88	1.25	0.77
4.	0.62	0.89	0.55
5.	0.48	0.70	
6.		0.56	

6.2 Dynamic loading

Dynamic loading is specified in terms of seismic and wind time histories. In both cases a linear time history analysis is carried out to obtain the required floor response histories. Two of the seismic time histories introduced in Chapter 4 were selected for the analysis; the Imperial Valley fault normal component and the Northridge fault parallel component. The Imperial Valley earthquake is applied along the X axis while the Northridge earthquake is applied along the Y axis of the cross-section.

Wind time history is generated from the NatHaz on-line wind simulator [18]. The simulator provides the velocity variation versus time and the mean velocity at a specified height and for a particular input value of the three second gust wind speed. For a height of 202m or 663ft (maximum height of the 52-story building) and a three second gust wind speed of 40m/s, the mean wind speed is added to the velocity variation at any given time to obtain the wind time history as represented in Figure 6.2.

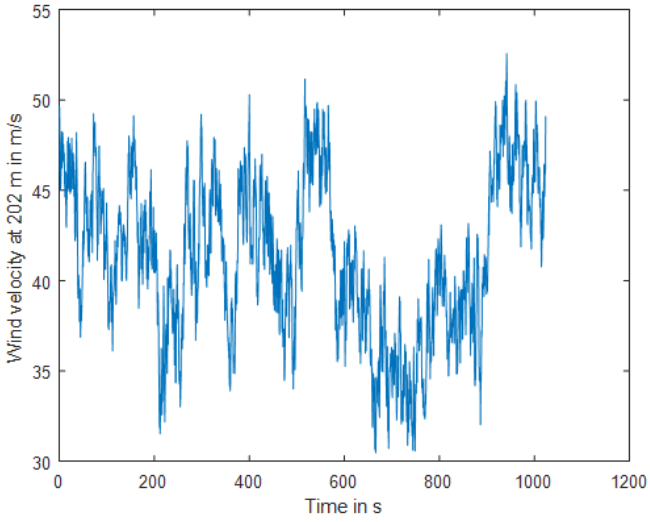

Figure 6.2 Wind velocity vs time

The corresponding equations used in the numerical simulations are as follows

$$u_{202}(t) = U + u_s(t) \tag{6.1}$$

where, $u_s(t)$ is the wind velocity variation (or standard deviation), *U* is the mean velocity and $u_{202}(t)$ represents the resulting time history, all at 202m. Since wind loads also change with height, the power law is used to model this dependence.

$$u(z) = u_{10}\left(\frac{z}{10}\right)^{\alpha_p} \tag{6.2}$$

where, u_{10} is the height at 10m, *z* is the specified height and the value of the exponent α_p is taken as *1/7* . Since the velocity at 202m is known, Eq (6.2) can be modified as

$$u(z) = u_{202}\left(\frac{z}{202}\right)^{\alpha_p} \tag{6.3}$$

Hence, the combined equation for wind velocity at any given time and height is taken as

$$u(t,z) = \left[U + u_s(t)\right]\left(\frac{z}{202}\right)^{\alpha_p} \tag{6.4}$$

In order to obtain the wind load, the wind velocity is converted into a uniformly distributed load applied along the length of each floor, using the equation of drag force as described in Eq (6.5)

$$f(t,z) = \frac{1}{2}\rho C_D u(t,z)^2 h \tag{6.5}$$

where, $f(t,z)$ is the uniformly distributed load, ρ is the density of air (1.2kg/m^3), C_D is the drag coefficient taken as 2.4 and *h* is the floor height (3.96m or 156ft).

In SAP 2000 [30], the uniformly distributed wind load as a function of time at 202m is specified as a time history function excluding the height variation. The applied time history is then scaled down in magnitude as described by the power law by specifying a stepped load pattern that decreases with height. A linear time history analysis is then carried out with the described loading. Figure 6.3 represents the stepped load pattern applied to the model along the X direction.

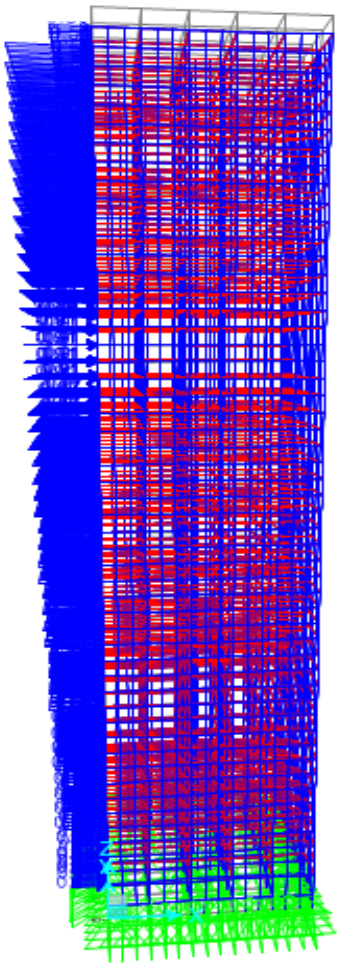

Figure 6.3 Stepped load pattern

6.3 Seismic response characterization

As previously mentioned, two cases are considered here to understand response characteristics under two different earthquake scenarios and extract translational modal parameters about both the XZ and YZ planes. Hence the Imperial Valley fault normal component is applied along the X direction (ivnx) to obtain X directional displacement response and recover modal characteristics along the XZ plane while the Northridge fault parallel component is applied along the Y direction to obtain Y directional displacement response and recover modal parameters along the YZ plane.

In order to quantify the requirement of sensors for the reconstruction process, a number of configurations are studied by selectively removing sensors from the initial assumption of one sensor per floor. Since 52 is a large number for sensor instrumentation, it is suggested to remove sensors ensuring uniform spacing between the remaining ones. The decision of uniform sensor spacing was considered after carrying out a mode shape reconstruction analysis with non-uniform sensor spacing, which yielded distorted modes. Also, since the response is inherently linear, uniform spacing makes it mathematically easier to interpolate missing information. Figure 6.4 shows the sensor configurations considered. The first configuration (27) has every other sensor removed, the second every two other, third every three other and so no until only the first and last sensors remain. It is important to definitely retain these two sensors as they define the range of the constructed mode shapes. This constraint leads to a maximum case of 27 and a minimum of two as opposed to considering all 52 sensors. Since 52 as

a number has very few factors and to accommodate the constraint of retaining the last sensor, the criteria for equal spacing is compromised on the last two sensors.

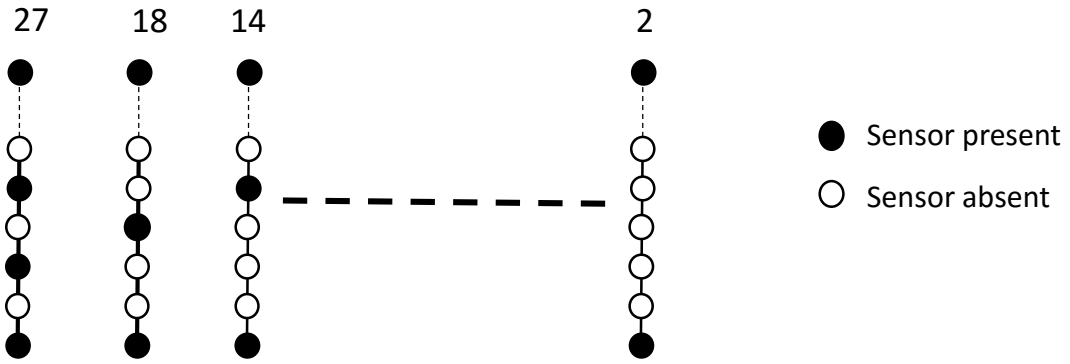

Figure 6.4 Sensor configurations

Since dynamic response is a product of its modal contribution factors and the contributing mode shapes, the TDD methodology is first carried out to obtain these parameters before the response reconstruction process. Only the first four modes (along the XZ and YZ planes for ivnx and nrpy respectively) are considered for this purpose. These are identified from the power spectral density functions of the responses and are used to design the digital filters to obtain mode isolated time histories. In order to facilitate the understanding of the impact of missing sensor information, only the extreme scenarios which are the 52, 27 and two sensor cases are presented below, other configurations are considered further in the analysis as required. Figures 6.5 and 6.6 show the modal contribution factors for the first four modes obtained from the TDD process for each of the two earthquake scenarios, shortly abbreviated as ivnx and nrpy.

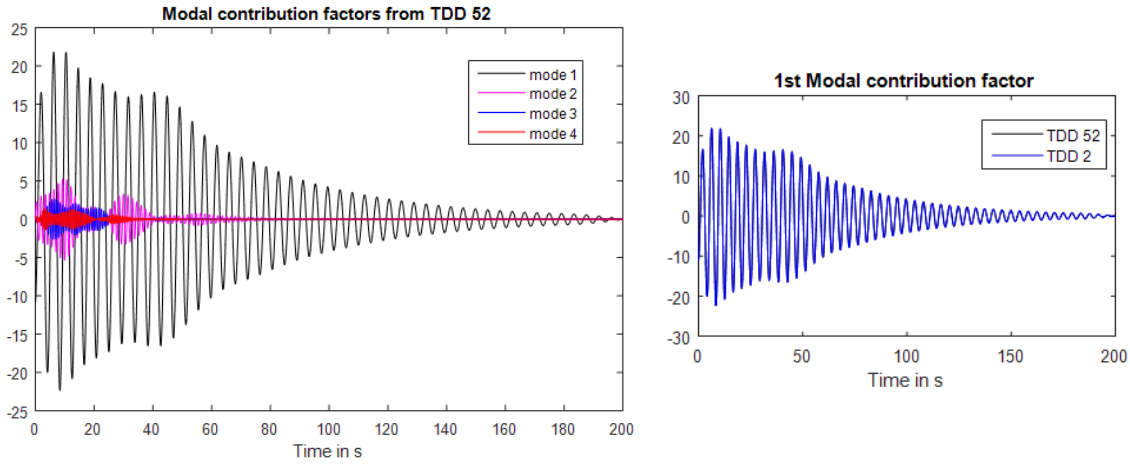

Figure 6.5 Modal contribution factors from ivnx

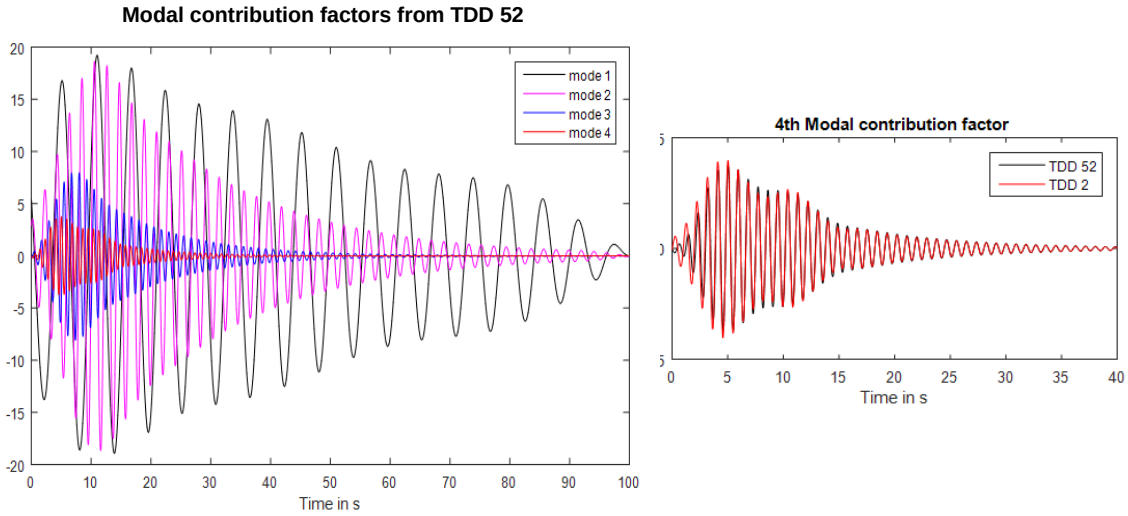

Figure 6.6 Modal contribution factors from nrpy

There are two critical observations from the above figures; the first of which pertains to the contribution from different modes and the other refers to the impact of reduced sensor data. Elaborating on the first observation, in case of ivnx, the contribution from the first mode is far greater than any other mode indicating that the

first mode shape alone might be sufficient to get reasonably accurate response reconstruction results. Similarly, in case of nrpy, as observed from Figure 6.6 the first two mode shapes have greater contribution than higher modes although the higher modal contribution is more significant than the case of ivnx. Here, the first two mode shapes may be adequate to capture the reconstructed responses however other modes could also impact its accuracy since their contribution is not negligible unlike the ivnx case. Moving on to the second observation, the two sensor case performs nearly as well as the 52 sensor case in capturing the time history. Even the fourth modal contribution is fairly accurate indicating the redundancy of 50 sensors for this analysis.

The MATLAB spline interpolation function is considered for interpolating the mode shapes, since the TDD process only provides as many data points as the number of floor responses given as input. Hence in case of 27 sensors, 27 is interpolated to 52 while it is two to 52 in the two sensor case. Figures 6.7 and 6.8 show the first three modes obtained from both the seismic responses along the XZ and YZ planes.

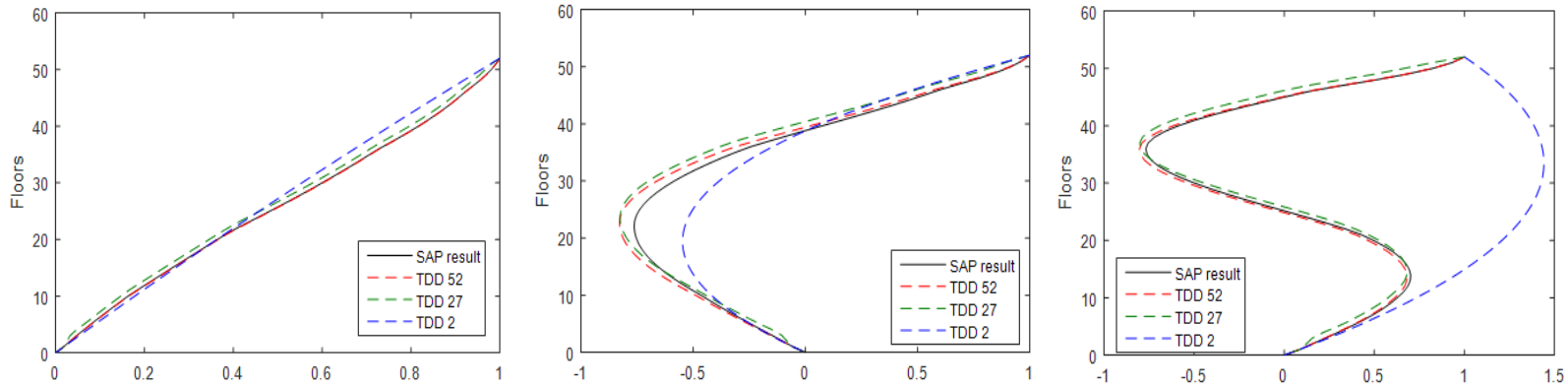

Figure 6.7 First three mode shapes on the XZ plane from ivnx

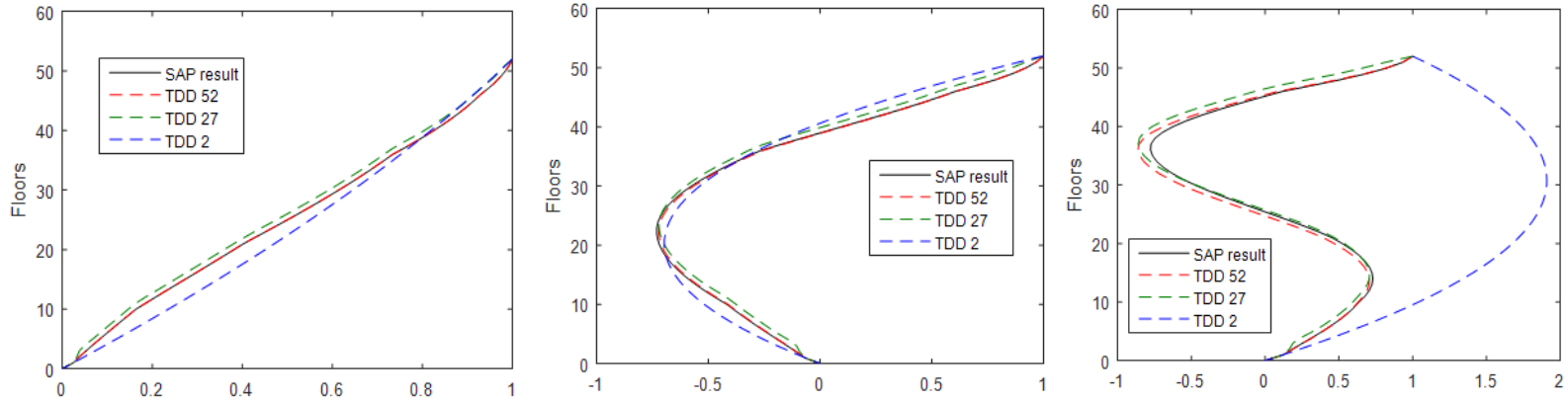

Figure 6.8 First three mode shapes on the YZ plane from nrpy

The above figures indicate that two sensors cannot capture more than two modes. With regards to accuracy, it is observed that the two-sensor case appears to perform as well as the higher sensor cases for the nrpy response while it displays some outliers in the second mode with the ivnx response. Hence, while the mode shape accuracy can be improved by adding more sensors, it is fair to state that the required number of sensors depends on the number of modes required to be captured. In case of ivnx, there is very little motivation for plotting higher modes due to the negligible values of the corresponding contribution factors. However with the nrpy case, it is of interest to know the number of sensors needed for constructing at least the first four mode shapes. Figure 6.9 satisfies this curiosity indicating that a minimum of five sensors are required to capture the first four modes while four sensors prove insufficient.

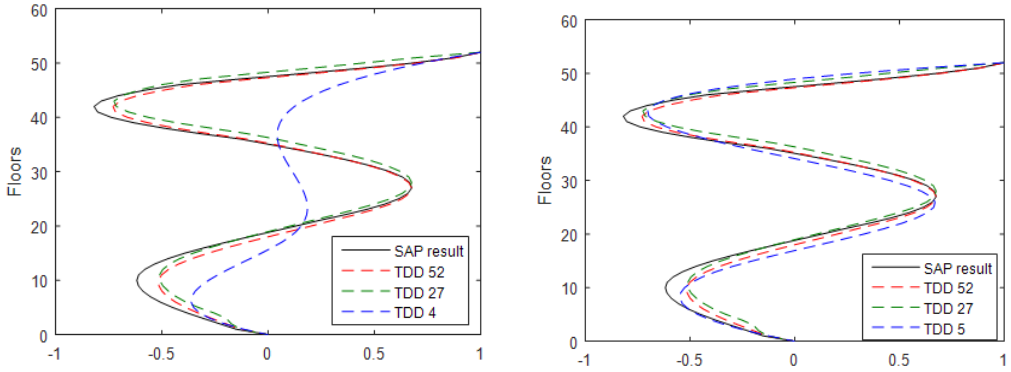

Figure 6.9 Fourth mode shape (YZ plane) from nrpy

An interesting aspect to be considered at this stage is sensor damage. It was earlier mentioned that equal spacing is important for accurate mode shape capture and

that there is a minimum sensor requirement for accurately capturing a specified number of modes. Under these circumstances, a larger number of equally spaced sensors is taken to start with and a certain number of sensors are randomly removed to observe the modal behavior. The objective of this analysis is to observe how a certain uniform sensor configuration behaves when some of its components get damaged randomly. In this analysis, a uniform sensor configuration with 11 sensors is chosen as being the maximum sensor case from the financial point of view for instrumenting a structure of this height. These sensors are assumed to be in a uniform distribution from which a 50% probability of failure is considered. Hence two cases are presented below. Case 1 where five sensors are randomly removed and Case 2 where six sensors are randomly removed from the 11 equally spaced sensor configuration. Mode shapes for the second and third modes are plotted in Figure 6.10 for the ivnx response considering both these cases (labeled TDD 11-5 and TDD 11-6 respectively) and their equivalent equally spaced counterparts TDD 6 and TDD 5.

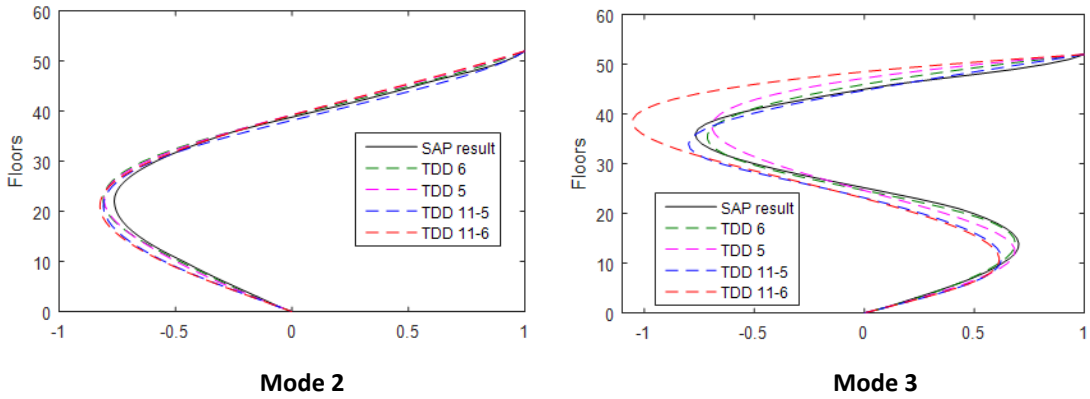

Figure 6.10 Random sensor removal on the XZ plane (from ivnx)

The same is repeated with the nrpy response. Two plots of the fourth mode shape are shown successively placed in Figure 6.11 the first pertaining to five sensor removal and TDD 6, and the second pertaining to six sensor removal and TDD 5. A plot of the second mode shape lies next to these graphs showing the performance of all these cases.

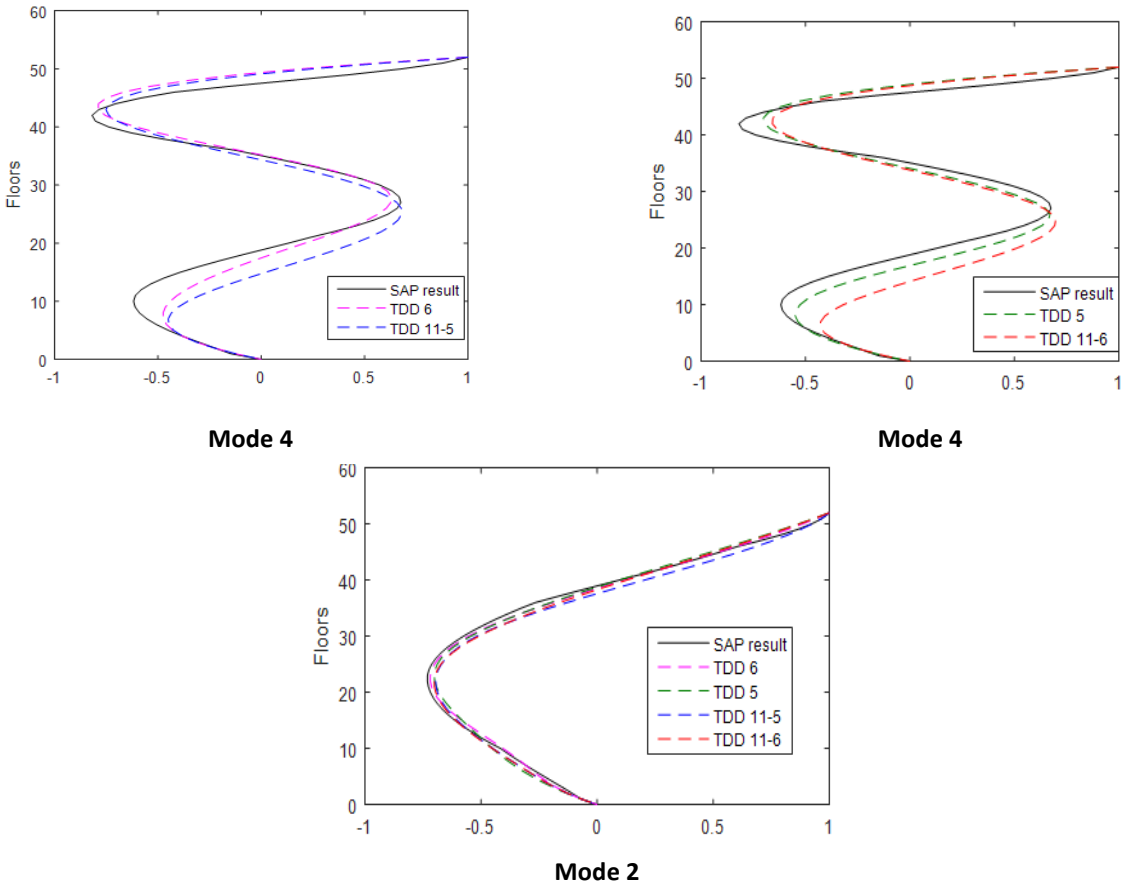

Figure 6.11 Random sensor removal on the YZ plane (from nrpy)

It is clearly observed that random sensor removal does not affect the accuracy of mode shapes if more than the minimum number of sensors are present for the mode to be

captured. Hence, the second mode is fairly accurate in both cases (TDD 11-5 and TDD 11-6) under both earthquake scenarios. The higher modes also appear reasonable but their performance can be improved by increasing the number of sensors.

Having obtained the modal parameters, response reconstruction is now carried out for the 27 and two sensor cases for every floor. The reconstruction results are presented in Figures 6.12 to 6.15 for the 50th and 20th floors both of which do not originally have sensors in either of the cases. It is to be noted that in case of 27 sensors, the first four modes are considered in the TDD process however for the two-sensor case only the first two modes are considered since it is unable to capture higher modes as described previously. The maximum values and root mean squared (RMS) errors are given in the tables below (Table 6.2 and 6.3) to aid the visual understanding.

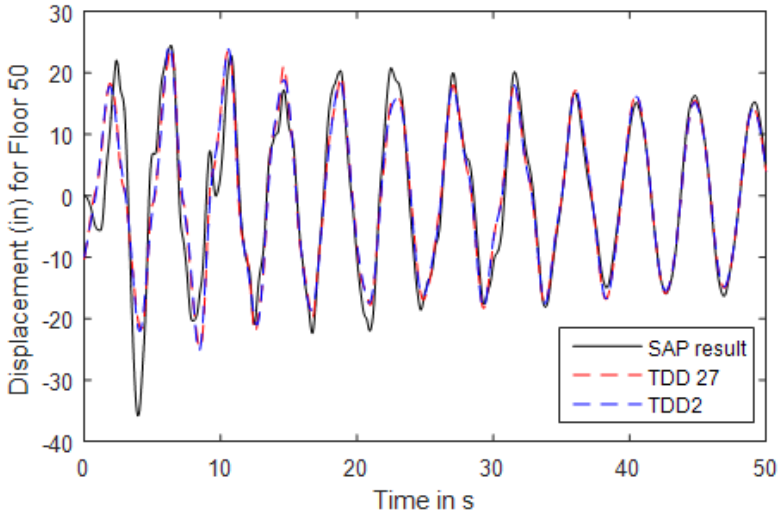

Figure 6.12 Response reconstruction for the 50th floor (ivnx)

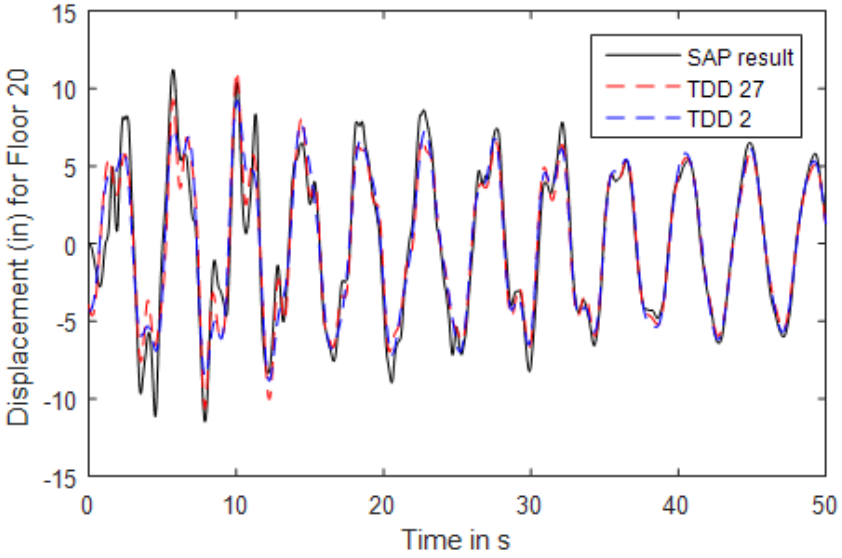

Figure 6.13 Response reconstruction for the 20th floor (ivnx)

Table 6.2 Maximum values and RMS errors (ivnx)

Floor	Maximum Values (in)			RMS Errors	
	SAP result	TDD 27	TDD 2	TDD 27	TDD 2
50	35.8096	24.7619	25.2557	2.0720	2.0927
20	11.4784	11.1258	9.2193	0.6756	0.7429

Results indicate that the performance of the two-sensor case is very similar to the 27-sensor case although it considers only two modes. This is primarily due to the high contribution of the first mode (as seen in Figure 6.5). It is also interesting to observe that the 20th floor has lesser errors than the 50th floor. An increase in the number of sensors or number of modes considered does not appear to impact the response very much, which is noticeably observed while comparing the maximum values in the 50th floor

(Table 6.2). A similar behavior is also observed with the nrpy response as presented below.

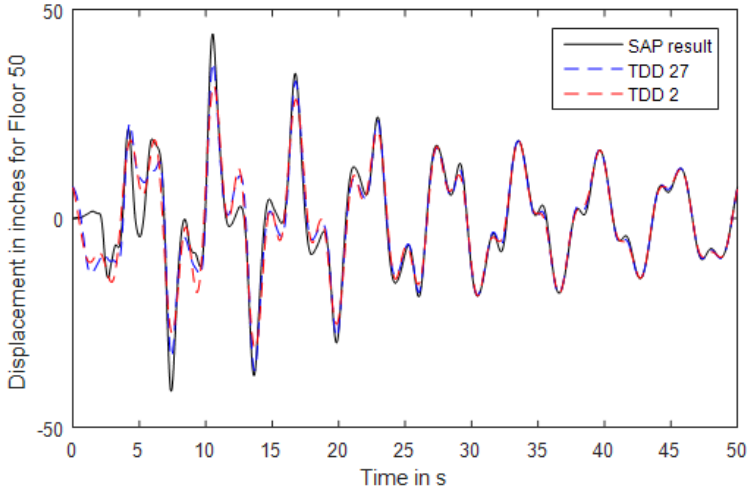

Figure 6.14 Response reconstruction for the 50th floor (nrpy)

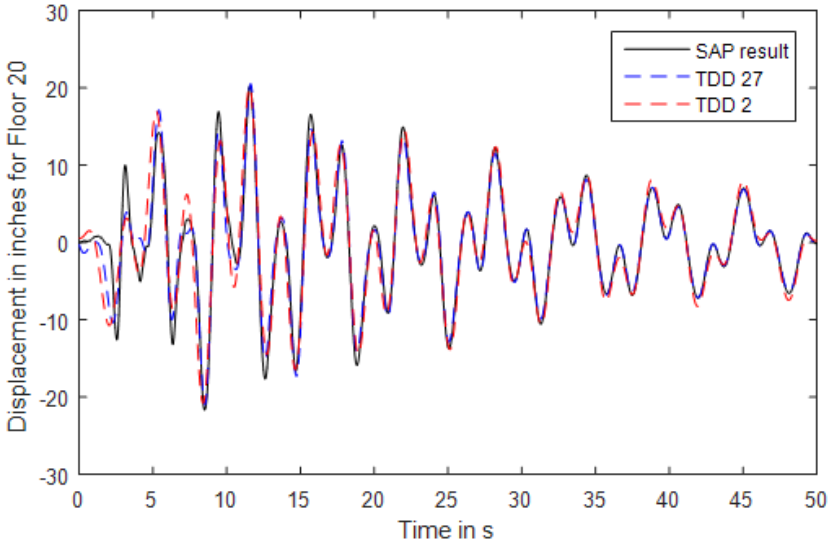

Figure 6.15 Response reconstruction for the 20th floor (nrpy)

Table 6.3 Maximum values and RMS errors (nrpy)

Floor	Maximum Values (in)			RMS Errors	
	SAP result	TDD 27	TDD 2	TDD 27	TDD 2
50	44.1492	37.2975	31.8272	2.6797	2.8868
20	21.6716	20.9956	20.7891	1.0723	1.7191

The TDD process generates reasonably accurate results with minimal sensors, however it is of interest to probe into a possible reason for the observed behavior of errors which is investigated below. On reviewing the equations associated with response reconstruction (Eq (3.17) and Eq (3.15)), it is observed that apart from the mode shapes, the filtered input responses are the only other variables involved. In order to eliminate the possibility of error in the first variable, first four mode shapes from the finite element results are used in Eq (3.15) to calculate the modal contribution factors and these factors are multiplied again with the same mode shapes to generate the reconstructed response for the ivnx case (Figure 6.16). It is to be noted that even then there is a root mean squared error of 2. 0675 for the 50^{th} floor while the error with two sensors was 2.0927. This clearly indicates that the second variable, the filtered response contributes more towards the error than the mode shapes. However, this does not completely explain the reason behind the reduction in errors with decrease in height, since it's the mode shapes that vary with height and not the modal contribution factors. Hence this analysis proposes an improvement in the design of the digital filter to be one of the methods to increase the accuracy of results.

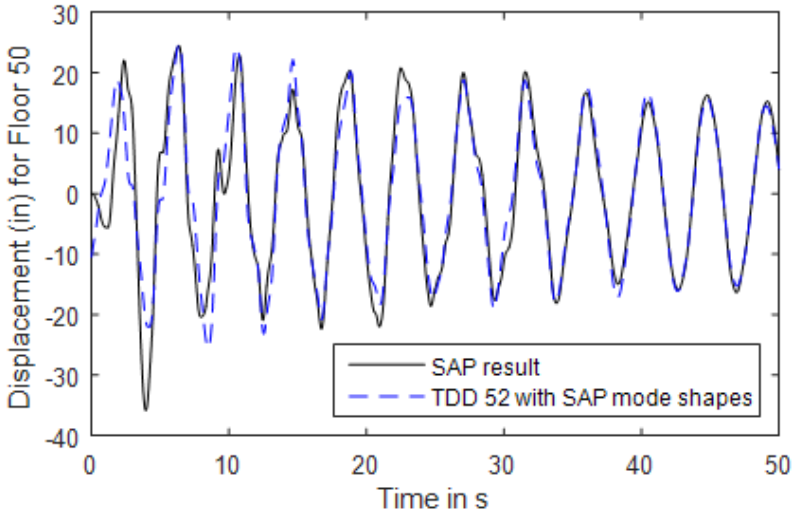

Figure 6.16 Response reconstruction with mode shapes from finite element analysis

6.4 Wind response characterization

For this analysis, wind loading is applied along the X direction and the translational modal features about the XZ plane are derived to perform the response reconstruction process. A plot of the power spectral density (PSD) of the X directional response is given in Figure 6.17 (a), the graph is further magnified twice to show the first three modes labelled as plots (b) and (c) in Figure 6.17 below.

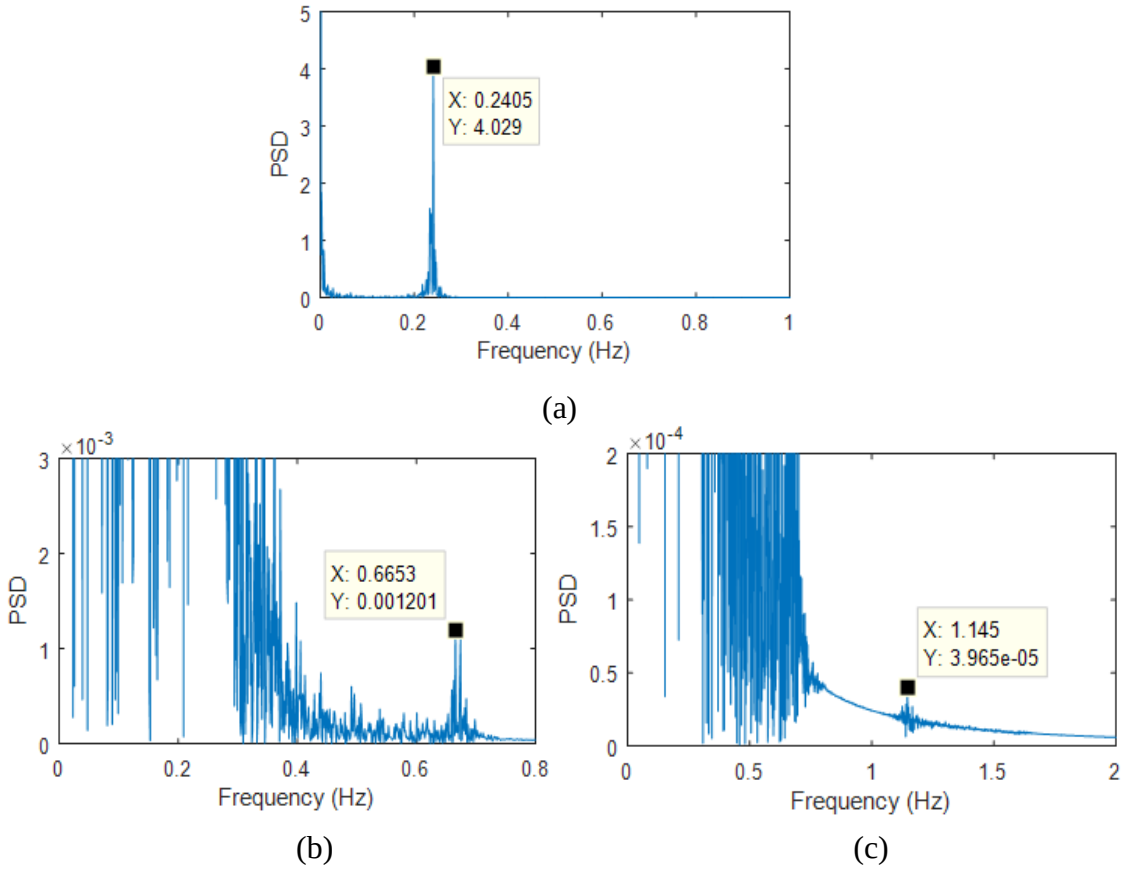

Figure 6.17 First three modes about XZ (wind)

Unlike the linear seismic responses where the building vibrates about its original position (or nearly zero displacement), the wind responses show building vibration about an initial finite displacement. Hence, zero frequency of the PSD graph is associated with a high power. It is also observed that there is a certain amount of low frequency content in the wind response occurring before the first mode. The graphs in general have more noise content than their seismic counterparts indicating that the modes obtained through the process may appear more distorted. The mode shapes and modal contribution factors obtained through the TDD approach are given in Figures 6.18 and 6.19 respectively. It

is interesting to note that the method is unable to capture higher modes even with all sensors in place.

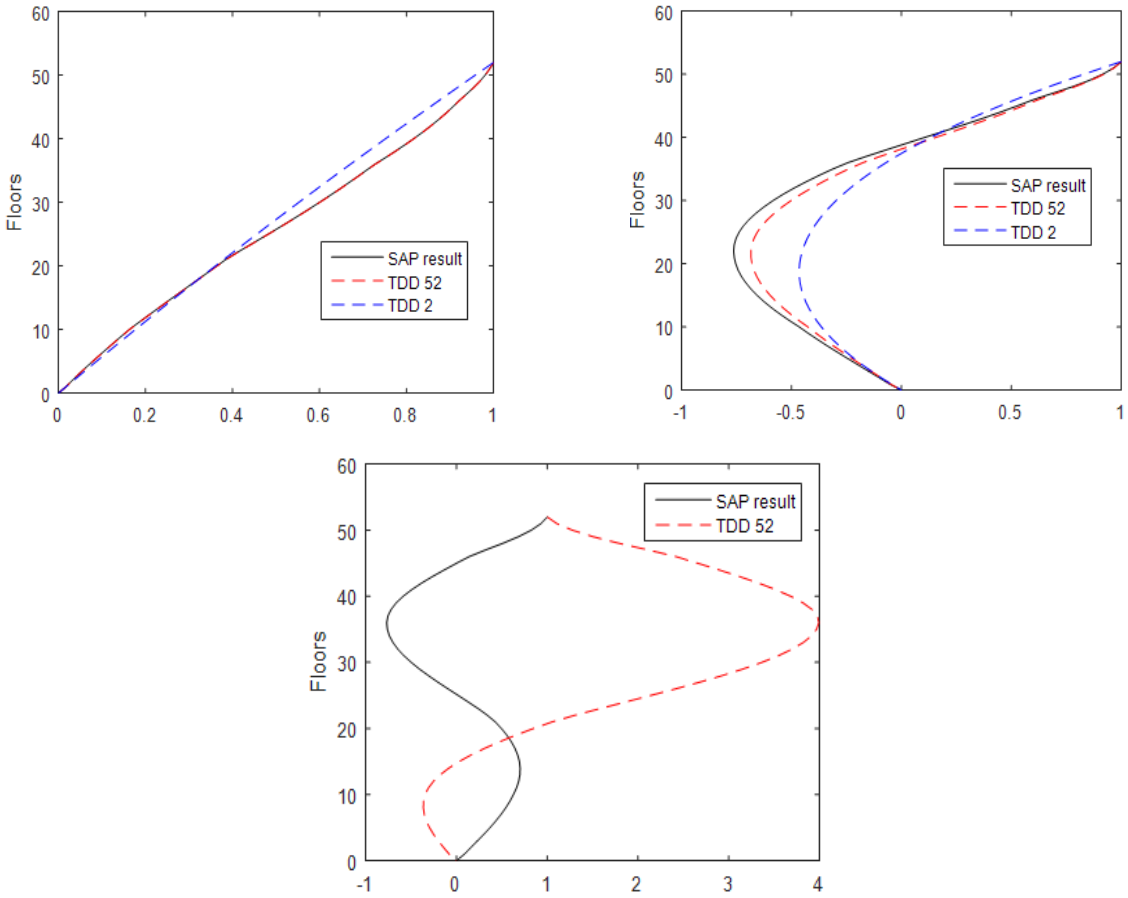

Figure 6.18 First three mode shapes about the XZ plane (wind)

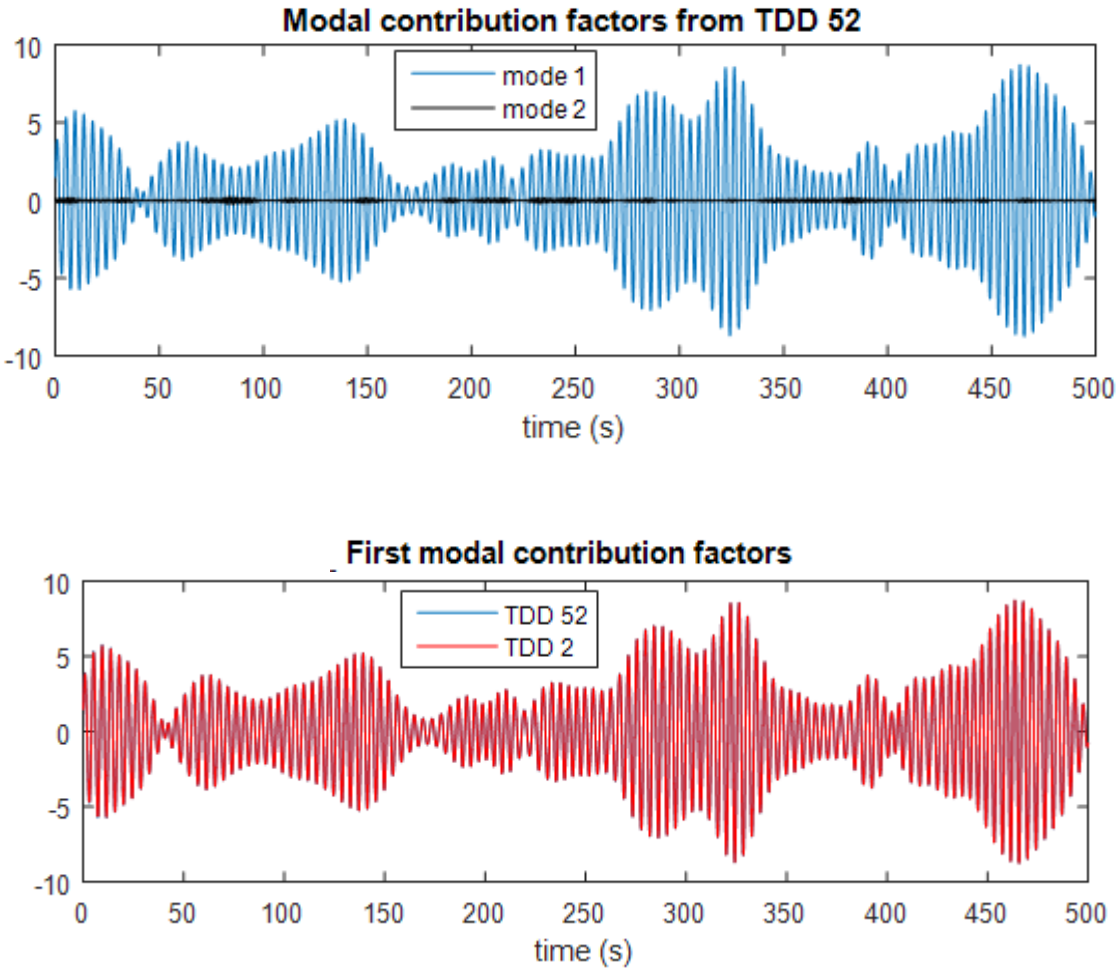

Figure 6.19 Modal contribution factors (wind)

The modal contribution factors show negligible change when more sensors are used also, the first modal contribution is much larger than the second mode. It can also be noticed that the mean of the time history is zero however it is not so for the input wind responses as the building vibrates about a finite displacement. Response reconstruction with two mode shapes gives the following results (Figure 6.20).

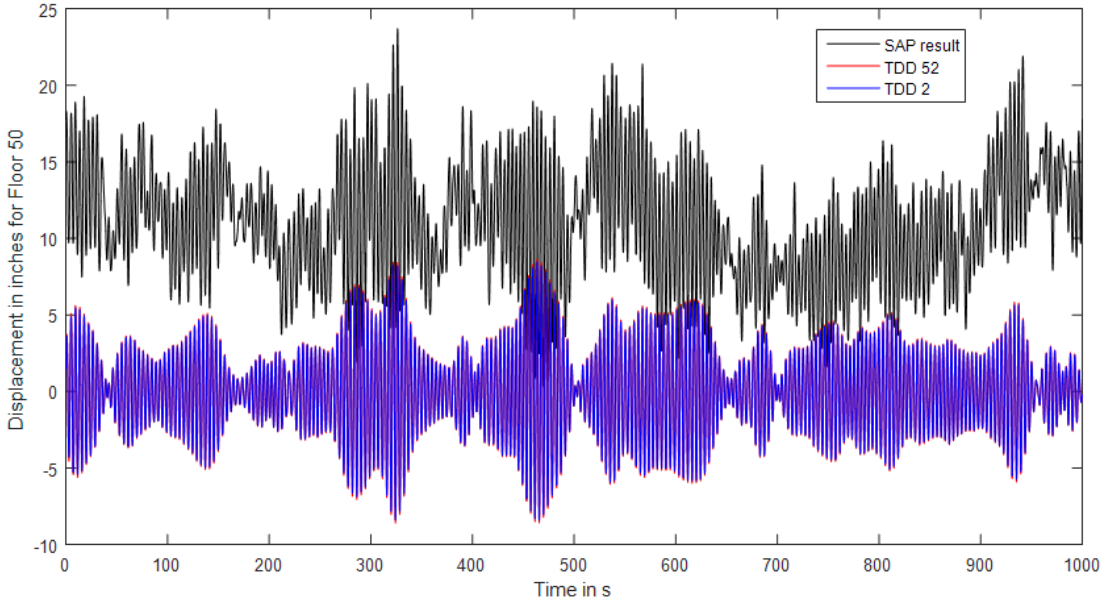

Figure 6.20 Response reconstruction for the 50th floor (wind)

As expected, the reconstruction process is not successful unlike the seismic case. However, this is mostly due to the reason that the underlying trend in the mean of the response is not captured in the reconstructed time series. The response variation appears to be reconstructed reasonably. This analysis brings out an inherent deficiency in the TDD methodology as the reconstruction process does not just depend on the reconstructed modal parameters but appears to have other contributing factors. A probable contributor could be the low frequency content of the response as observed in its power spectral density function (Figure 6.17 (a)). This aspect can be addressed as future work to improve the methodology.

7. SUMMARY AND CONCLUSIONS

The major objective of this research study was to investigate a subset of multi-hazard dynamic loading on the response of multi-storied structures with a focus on modal extraction and response reconstruction. In order to better appreciate this objective three tasks are identified and performed. First the open literature was studied in order to better understand current trends in sensor technology that could be applied to sensor placement and structural control strategies. Second, the Time Domain Decomposition (TDD) method was used to investigate the modal parameters derived from the seismic response of a 20-story building. Third, the TDD methodology was used to investigate and characterize the seismic and wind response of an idealized 52-story building with regards to time series response reconstruction subject to missing sensor information. The thesis research results presented are restricted to linear response behavior that incorporated finite element models using SAP 2000 [30].

Several key conclusions have been derived through the course of this research concerning characteristics of the dynamic response, the ideal number and placement of sensors and application of the TDD methodology. Both wind and seismic loads are found to excite nearly similar modal frequencies, however on comparing their response histories some prominent differences are observed. Since only linear seismic responses are considered, no permanent deformations are observed and hence the building vibrates about its original position producing a nearly constant zero mean in its response history. This is quite unlike the nature of the linear wind responses that have an initial static

displacement and the building may not necessarily vibrate about that static response throughout its history, hence displaying an underlying trend in the non-zero mean of its response history. Also, seismic loading has a much shorter duration (about 15-40s) than its actual response history (plotted for about 100-200s). Thus, the bulk of the generated response behavior is the result of free vibration decay, while response due to the excitation is restricted to the initial loading period. The response history appears very harmonic beyond the duration of its loading history and can be filtered into single degree of freedom signals using common digital filters. The wind response on the other hand is plotted for nearly the exact duration of its loading history since the loading history is long (about 1000s) and is not transient in nature. The resulting response thus appears less harmonic as it is mostly characterized by the forcing function, and a digital bandpass filter proves insufficient to obtain its single degree of freedom response.

With regards to sensor placement it was found that uniform sensor placement is, not surprisingly, the most ideal for the linear models. Building response due to higher vibrational modes can be captured with the introduction of additional sensors as per the TDD methodology, however for linear seismic responses significant modal contributions are not observed beyond the first few modes. Thus, very satisfactory response reconstruction results were obtained for the seismic loading cases with just two sensors placed at the lowest and highest floors of the building. The placement methodology also appeared tolerant towards random sensor removal, which might be due to sensor damage or lack of power during natural disasters. The wind response characterization revealed some deficiencies within the TDD methodology. The TDD reconstruction process did

not accurately capture the underlying trend in the mean of the response and could not capture higher modal behavior in this case. Based on this research further study into the modification of the modal based filter might result in improved performance in capturing the underlying trend in the mean for the wind responses and perhaps improve the general accuracy of the seismic response reconstruction results.

REFERENCES

[1] Al-Saffar, Y., Aldraihem, O., and Baz, A. (2012). "Smart paint sensor for monitoring structural vibrations." *Smart Materials and Structures*, 21(4), 045004.

[2] Anonymous "Prudential Tower " http://labicenter.org/picsowc/Prudential-Tower.html (5/31/2016, 2016).

[3] Anonymous "Suites of Earthquake Ground Motions for Analysis of Steel Moment Frame Structures." http://nisee.berkeley.edu/data/strong_motion/sacsteel/ground motions.html 2015).

[4] Anonymous "The Skyscraper Center " http://www.skyscrapercenter.com/ (5/31/2016, 2016).

[5] ASCE. (2005). "Minimum design loads for building and other structures." *ASCE 7–05*, New York.

[6] Bonello, P., Rafique, S., and Shuttleworth, R. (2012). "A theoretical study of a smart electromechanical tuned mass damper beam device." *Smart Materials and Structures*, 21(12), 125004.

[7] Cazzulani, G., Resta, F., Ripamonti, F., and Zanzi, R. (2012). "Negative derivative feedback for vibration control of flexible structures." *Smart Materials and Structures*, 21(7), 075024.

[8] Fang, S. M., Niedzwecki, J. M., Fu, S., Li, R., and Yang, J. (2014). "VIV response of a flexible cylinder with varied coverage by buoyancy elements and helical strakes." *Marine Structures,* 39 70-89.

[9] Gagliardi, G., Salza, M., Ferraro, P., De Natale, P., Di Maio, A., Carlino, S., De Natale, G., and Boschi, E. (2008). "Design and test of a laser-based optical-fiber Bragg-grating accelerometer for seismic applications."*Measurement Science and Technology,* 19(8), 085306.

[10] Gelfuso, M. V., Thomazini, D., Souza, Júlio César Silva de, and Lima Junior, José Juliano de. (2014). "Vibrational analysis of coconut fiber-PP composites." *Materials Research,* 17(2), 367-372.

[11] Gonzalez-Buelga, A., Clare, L., Neild, S., Burrow, S., and Inman, D. (2015). "An electromagnetic vibration absorber with harvesting and tuning capabilities." *Structural Control and Health Monitoring,* 22(11), 1359-1372.

[12] Górriz, B. T., García, P. C., Payá-Zaforteza, I. J., and Maicas, S. S. (2014). "Experimental and numerical analysis of a hybrid FBG long gauge sensor for structural health monitoring." *Measurement Science and Technology,* 25(12), 125107.

[13] Gupta, A., and Krawinkler, H. (1999). "Seismic demands for performance evaluation of steel moment resisting framed structure". Doctorate. The Leland Stanford Junior University.

[14] Gur, S., Roy, K., and Mishra, S. K. (2015). "Tuned liquid column ball damper for seismic vibration control." *Structural Control and Health Monitoring*, 22(11), 1325-1342.

[15] Hurlebaus, S., "CVEN 695 Frontiers in Civil Engineering". Presentation.

[16] Kim, B. H., Stubbs, N., and Park, T. (2005). "A new method to extract modal parameters using output-only responses." *Journal of Sound and Vibration*, 282(1), 215-230.

[17] Kim, K., and Kim, J. (2015). "Dynamic displacement measurement of a vibratory object using a terrestrial laser scanner." *Measurement Science and Technology*, 26(4), 045002.

[18] Kwon, D., and Kareem, A. (2006). "NatHaz on-line wind simulator (NOWS) : simulation of Gaussian multivariate wind fields." *NatHaz Modeling Laboratory Report*, Univ. of Notre Dame, http://windsim.ce.nd.edu/.

[19] Laflamme, S., Slotine, J. E., and Connor, J. (2012). "Self-organizing input space for control of structures." *Smart Materials and Structures*, 21(11), 115015.

[20] Lee, J., Ho, H., Shinozuka, M., and Lee, J. (2012). "An advanced vision-based system for real-time displacement measurement of high-rise buildings." *Smart Materials and Structures*, 21(12), 125019.

[21] Liao, W., Wang, J., Song, G., Gu, H., Olmi, C., Mo, Y., Chang, K., and Loh, C. (2011). "Structural health monitoring of concrete columns subjected to

seismic excitations using piezoceramic-based sensors." *Smart Materials and Structures,* 20(12), 125015.

[22] Mascarenas, D. D., Flynn, E. B., Todd, M. D., Overly, T. G., Farinholt, K. M., Park, G., and Farrar, C. R. (2010). "Development of capacitance-based and impedance-based wireless sensors and sensor nodes for structural health monitoring applications." *Journal of Sound and Vibration,* 329(12), 2410-2420.

[23] Meng, D., and Ansari, F. (2013). "Damped fiber optic low-frequency tiltmeter for real-time monitoring of structural displacements." *Measurement Science and Technology,* 24(12), 125106.

[24] Niedzwecki, J. M., and Fang, S. M. (2013). "Hydrodynamic response behavior of ribbon fairing." *Oceans-San Diego, 2013,* IEEE, 1-4.

[25] Niedzwecki, J. M., and Fang, S. (2013). "Suppression of flow-induced vibrations using ribbon fairings." *International Journal of Computational Methods and Experimental Measurements,* 1(4), 395-405.

[26] Oh, B. K., Hwang, J. W., Lee, J. H., Kim, Y., and Park, H. S. (2015). "A strain measurement model using a limited number of sensors for steel beam structures subjected to uncertain loadings." *Measurement Science and Technology,* 26(11), 115007.

[27] Parker, D., and Wood, A. (2013). *The Tall Buildings Reference Book.* Routledge.

[28] Pnevmatikos, N. G., and Thomos, G. C. (2014). "Stochastic structural control under earthquake excitations." *Structural Control and Health Monitoring,* 21(4), 620-633.

[29] Qiu, Z., Wu, J., and Yuan, S. (2011). "A wireless sensor network design and evaluation for large structural strain field monitoring." *Measurement Science and Technology,* 22(7), 075205.

[30] SAP 2000 Version 17.3.0 [Computer Software].

[31] Sarkisian, M. (2016). *Designing tall buildings: structure as architecture.* Routledge.

[32] Somerville, P. G. (1997). *Development of ground motion time histories for phase 2 of the FEMA/SAC steel project.* SAC Joint Venture.

[33] Sun, Z., Li, B., Dyke, S. J., Lu, C., and Linderman, L. (2016). "Benchmark problem in active structural control with wireless sensor network." *Structural Control and Health Monitoring*, 23(1), 20-34.

[34] Wang, J., Law, S., and Yang, Q. (2014). "Sensor placement method for dynamic response reconstruction." *Journal of Sound and Vibration,* 333(9), 2469-2482.

[35] Wang, X., Wei, G., and Sun, J. (2013). "Sample selection based on kernel-subclustering for the signal reconstruction of multifunctional sensors." *Measurement Science and Technology*, 24(2), 025102.

[36] Young, B. S., "Tall Building Aerodynamics". Presentation.

[37] Zhang, C., and Xu, Y. (2016). "Optimal multi-type sensor placement for response and excitation reconstruction." *Journal of Sound and Vibration*, 360 112-12.